In presenting the dissertation as a partial fulfillment of the requirements for an advanced degree from the Georgia Institute of Technology, I agree that the Library of the Institute shall make it available for inspection and circulation in accordance with its regulations governing materials of this type. I agree that permission to copy from, or to publish from, this dissertation may be granted by the professor under whose direction it was written, or, in his absence, by the Dean of the Graduate Division when such copying or publication is solely for scholarly purposes and does not involve potential financial gain. It is understood that any copying from, or publication of, this dissertation which involves potential financial gain will not be allowed without written permission.

3/17/65
b

ULTRAVIOLET OPTICAL PROPERTIES OF THE THALLIUM HALIDES

A THESIS

Presented to

The Faculty of the Graduate Division

by

David Chandler Hinson

In Partial Fulfillment

of the Requirements for the Degree

Doctor of Philosophy

in the School of Physics

Georgia Institute of Technology

November, 1966

ULTRAVIOLET OPTICAL PROPERTIES OF

THE THALLIUM HALIDES

Approved:

Date approved by Chairman: Dec. 7, 1966

ACKNOWLEDGMENTS

The author wishes to express his deep appreciation to Dr. James R. Stevenson for his suggestion of this research problem and for his personal guidance and assistance during the research. He is also indebted to Dr. Augustus L. Stanford and Dr. Peter B. Sherry for their critical reading of the manuscript. The encouragement and support of the faculty of the School of Physics is gratefully acknowledged.

The construction of equipment for this research was aided by a grant from the National Science Foundation.

TABLE OF CONTENTS

LIST OF TABLES

LIST OF ILLUSTRATIONS

LIST OF ILLUSTRATIONS

SUMMARY

The optical properties of thallium chloride and thallium bromide have been determined in the 3 ev to 21.2 ev region of the electromagnetic spectrum. These ionic crystals have a dielectric constant intermediate between the alkali halides and many semiconductors. Since many of the electronic and optical properties of a material are closely related to its dielectric constant, the choice of thallium chloride and thallium bromide provided materials for a study of optical properties with an intermediate value for the dielectric constant. In addition these materials have been the subject of frequent infrared investigations but have been neglected in the vacuum ultraviolet.

Coincident with this study of the optical properties of the thallium halides an evaluation was made of the two major methods used at present for determining the optical constants of a material from its reflectivity properties. These two methods are a graphical analysis of the reflectivity as a function of angle of incidence, and a Kramers-Kronig dispersion analysis. The reflectivity data were analyzed using both methods and the results compared. A third independent method of calculating optical constants was used, in which experimental data on the reflectivity as a function of the angle of incidence of the light on the sample were fitted to the appropriate Fresnel curve by a computer. The parameters n, k, and the polarization of the incident light were varied to choose the proper curve. This latter method avoided the approximations and extrapolations of the other two methods but is more difficult experimentally.

A major part of the experimental effort was the design and construction of a monochromator to operate from the visible to the vacuum ultraviolet region of the electromagnetic spectrum. The design considerations also included an appropriate sample chamber for studying the reflectivities of crystals as a function of angle of incidence and an evaluation of light detectors. The monochromator was a one-meter, normal incidence, vacuum ultraviolet type which covered the wavelength range from 600 Å to 6000 Å. The light source was a McPherson Hinteregger-type gas discharge lamp. It was operated in a dc mode using hydrogen or helium, or as a capacitor discharge in helium to cover the desired range. The capacitor discharge in helium has never been used previously as a light source for reflectivity measurements, but it gave satisfactory results for this research. The incident reflected light intensities were determined by means of a photomultiplier tube outside the sample chamber. The ultraviolet light was converted to visible light, to which the photomultiplier tube was sensitive, by a sodium salicylate phosphor. The fluorescence of this phosphor was transmitted to the photomultiplier tube by means of an aluminum-coated solid Pyrex light-pipe. The state of polarization of light from the exit slit of the monochromator was measured using a LiF pile-of-plates analyzer.

The reflectivities of TlCl and TlBr were determined in the range 3.0 ev to 21.2 ev for incidence angles of 20° and 70°. These reflectivities were used to determine n and k for the materials by a graphical method, and the 20° reflectivity was used in a Kramers-Kronig analysis of the data. The results of the two methods agreed well at high energies, but differences as large as 100 per cent were found at

low energies where n and k were large. The results of the Fresnel curve-fitting technique on TlBr indicated that the Kramers-Kronig technique was correct to within 15 per cent, but that the polarization of the incident light caused large errors in a graphical analysis of the data unless the polarization was taken into account.

The complex dielectric constant and the electron energy loss function were calculated from n and k for both materials and used in interpreting the optical properties in terms of electronic transitions in the material. The low-energy results were in accord with transmission work done previously on these materials in this region. The first absorption band consists of an exciton peak, weak in TlBr, and an underlying absorption edge for band-to-band transitions. From the behavior of the dielectric constant at the absorption edge in TlBr, the band gap has been determined to be 3.05 ev. Interpretation of the remaining peaks was uncertain due to the absence of energy band calculations on these materials.

The existence of a plasma resonance peak in the energy loss function has been tentatively identified at 11.8 ev for TlBr and at 12.4 ev for TlCl. These values agree closely with the corresponding values of 13.5 ev and 13.9 ev calculated for eight electrons per molecule free to perform collective oscillation in the conduction band. This electron density would be expected by considering the atomic energy levels of thallium, chlorine, and bromine. The 6s band of the Tl^+ ion, containing two electrons per molecule, and the 4p or 3p band of Br^- or Cl^-, respectively, containing six electrons per molecule, lie within 5 ev of the conduction band, while the next lower lying level is at least 15 ev below the conduction band.

CHAPTER I

INTRODUCTION

The Optical Constants

In a study of the interaction of optical radiation with matter, a knowledge of the optical constants of a material, more specifically its index of refraction and absorption index, is helpful. These constants describe the interaction of electromagnetic radiation with the material. Not only is a knowledge of the constants useful in engineering applications, but the energy dependence of the constants can aid greatly in a study of the physical mechanisms by which the interaction of radiation with matter occurs.

The consideration of a plane-polarized electromagnetic wave travelling in the $+x$ direction will serve to define the optical constants of the medium:

$$\vec{E}(x, t) = \vec{E}_o e^{-\frac{\alpha x}{2}} e^{i\omega(t - \frac{n}{c} x)} . \qquad (1)$$

In equation 1, α is the absorption coefficient describing the decrease in intensity of the electromagnetic radiation as it passes through the material, and n is the ordinary refractive index of the material, equal to the ratio of the velocity of propagation of the radiation in a vacuum to its velocity in the medium. Since electromagnetic radiation is a transverse wave the above expression would represent an electric field confined to a particular line in the y-z plane if $\vec{E}_o$ is

independent of time. If the component of $\vec{E}_o$ in the y direction were zero the wave would be linearly or plane-polarized in the z direction. The expression can be rewritten

$$\vec{E}(x, t) = \vec{E}_o \, e^{i\omega(t - \frac{1}{c}[n - \frac{i\alpha c}{2\omega}]x)}$$

$$= \vec{E}_o \, e^{i\omega(t - \frac{n'}{c}x)} , \qquad (2)$$

in which $n' = n - \frac{i\alpha c}{2\omega} = n - ik$ is the complex index of refraction of the material. Thus k is a measure of the absorption of the medium, and is known as its absorption index. If plotted as a function of energy it will show structure at energies for which strong absorption of radiation occurs, for example in the excitation of electrons between energy levels in a material.

The optical properties of a material can also be expressed in terms of its complex dielectric constant

$$\varepsilon' = n'^2 = \varepsilon_1 + i\varepsilon_2 . \qquad (3)$$

A plot of ε_1 and ε_2 as a function of energy can give information not only on the energy for which absorption occurs but also on the type of transition that occurs. For example when an absorption due to an electronic transition between discrete energy levels occurs, ε_1 and ε_2 exhibit "oscillator-like" behavior (1). This behavior is characterized by sharp peaks in ε_1 and ε_2 with ε_1 peaking slightly before ε_2. ε_1 would also exhibit the characteristic anomolous dispersion associated with the absorption of electromagnetic radiation by a charge oscillating

with a discrete frequency. If the absorption is due to an electronic transition between energy bands a calculation by Korovin (2) has shown that ε_1 exhibits a peak at an energy corresponding to the beginning of the band-to-band transition, while ε_2 rises steeply from zero to a constant value as is characteristic of a band edge.

The most straight-forward method of determining the optical constants of a material make use of the radiation transmitted by the material. This technique works well when the absorption coefficient α is less than 10^3 cm^{-1}. In the ultraviolet region of the spectrum, however, absorption coefficients as large 10^6 cm^{-1} can occur. The absorption coefficients are so large that the optical constants can not be measured by using transmitted light unless extremely thin samples of the materials are used. The optical properties of a thin film may differ greatly from those of the bulk material, however, and to determine the optical properties of single crystals or bulk material other techniques must be employed.

Another property of a material that depends sensitively on its optical constants, and can be used to calculate them, is the reflectivity. Until recently optical instrumentation had not been advanced enough to allow a detailed study of reflectivities of many materials in the vacuum ultraviolet region. With recent advances in vacuum systems, light sources, and radiation detectors, the reflectivities of many materials in this region have been examined and used to calculate their optical constants (3).

The fundamental equations governing the reflection of unpolarized radiation from a semi-infinite, homogeneous plane surface are the Fresnel

equations (See Appendix A)

$$r_s = \frac{\sin^2(\varphi + \chi)}{\sin^2(\varphi - \chi)} \quad \text{and} \quad r_p = \frac{\tan^2(\varphi + \chi)}{\tan^2(\varphi - \chi)} \,. \tag{4}$$

In the above equations r_s is the ratio of the intensity of the component of the reflected light polarized perpendicular to the plane of incidence to the intensity of the incident light. The plane of incidence is defined as the plane containing the incident and reflected rays. r_p is the corresponding ratio for the component polarized parallel to the plane of incidence. φ is the angle of incidence of the light at the surface and χ is the angle of refraction. The relation between φ and χ is provided by Snell's Law,

$$\sin \varphi = n' \sin \chi \,, \tag{5}$$

in which n' denotes the refractive index of the surface material. In an absorbing medium the refractive index is complex, and the angle of refraction χ becomes complex. A complex cosine can be introduced by the relation

$$n' \cos \chi = (n'^2 - \sin^2 \varphi)^{1/2} = a - ib \,. \tag{6}$$

If this relation is substituted into the Fresnel equations, they become

$$r_s = \frac{a^2 + b^2 - 2a \cos \varphi + \cos^2 \varphi}{a^2 + b^2 + 2a \cos \varphi + \cos^2 \varphi} \tag{7}$$

and

$$r_p = \frac{a^2 + b^2 - 2a \sin \varphi \tan \varphi + \sin^2 \varphi \tan^2 \varphi}{a^2 + b^2 + 2a \sin \varphi \tan \varphi + \sin^2 \varphi \tan^2 \varphi} \,. \tag{8}$$

The expressions for $a^2 + b^2$ and a in terms of n, k, and φ are:

$$a^2 + b^2 = \frac{1}{2}\left[n^2(1 - k^2) - \sin^2\varphi\right] + \frac{1}{2}\left\{\left[n^2(1 - k^2) - \sin^2\varphi\right]^2 + 4n^4k^2\right\}^{1/2} + \frac{2n^4k^2}{\left[n^2(1 - k^2) - \sin^2\varphi\right] + \left\{\left[n^2(1 - k^2) - \sin^2\varphi\right]^2 + 4n^4k^2\right\}^{1/2}} \tag{9}$$

and

$$2a = \left(\frac{1}{2}\left[n^2(1 - k^2) - \sin^2\varphi\right] + \frac{1}{2}\left\{n^2(1 - k^2) - \sin^2\varphi\right]^2 + 4n^4k^2\right\}^{1/2}\Bigg)^{1/2} . \tag{10}$$

In this way, the reflectances are expressed as functions of n, k, and the angle of incidence. These equations cannot be solved explicitly for n and k as a function of r_s, r_p, and φ. Consequently graphical methods of solution or simplifying approximations must be employed.

The Kramers-Kronig Method

One simplifying approximation occurs if near-normal incidence ($\varphi = 0$) light is used. Then the Fresnel equations assume the particularly simple form

$$r_p = r_s = \frac{(n' - 1)^2}{(n' + 1)^2} = \frac{(n - ik - 1)^2}{(n - ik + 1)^2} = |\tilde{r}|e^{i\theta}, \tag{11}$$

where $|\tilde{r}|$ is the amplitude of the complex reflectivity, and θ is the change in phase of the light wave that occurs upon reflection at the surface. The amplitude of the reflectivity is related to the measured reflection coefficient R, the ratio of the reflected light intensity

to the incident intensity, by the following:

$$R = \vec{r}^{\,*}\vec{r} = |\vec{r}|^2, \quad \text{so} \quad |\vec{r}| = \sqrt{R}, \tag{12}$$

a quantity which can be determined experimentally.

Equation (11) can be solved explicitly for n and k in terms of $|\vec{r}|$ and θ, resulting in

$$n = \frac{1 - |\vec{r}|}{1 + |\vec{r}| - 2|\vec{r}| \cos\theta} \tag{13}$$

and

$$k = \frac{-2|\vec{r}| \cos\theta}{1 + |\vec{r}| - 2|\vec{r}| \cos\theta} . \tag{14}$$

θ can be determined at a given frequency by employing the Kramers-Kronig relation from dispersion analysis (3), which gives

$$\theta(\omega_o) = \frac{1}{\pi} \int_0^\infty \ell n \left| \frac{\omega + \omega_o}{\omega - \omega_o} \right| \frac{d}{d\omega} \ell n \, |\vec{r}(\omega)| \, d\omega . \tag{15}$$

Thus by determining the complete reflectivity spectrum of a material for normal-incidence light, the optical constants can be calculated exactly.

Experimentally the complete reflection spectrum would be quite hard to determine, but only those parts of the spectrum near the region of interest contribute greatly to the optical constants in that region because of the weighting factor $\ell n \left| \frac{\omega + \omega_o}{\omega - \omega_o} \right|$ in equation (15). Also in those regions in which the reflectivity is changing smoothly with frequency, the reflectivity can be extrapolated from known regions of the spectrum. This extrapolation is of necessity quite arbitrary, and can

lead to fairly large errors in the optical constants determined from it (4), (5), particularly for energies near the extrapolated region.

Another approximation that is necessary due to geometrical considerations is that normal incidence light cannot be used, and "near-normal incidence" light, usually less than 20°, is used as an approximation to normal incidence. This approximation may also lead to errors, particularly if polarized light is used. For the typical values $n = 2$, $k = 1$, and 15 per cent polarization of the light, the difference between normal incidence reflectivity and 20° reflectivity is 1 per cent. For larger values of n and k and a greater degree of polarization, the error would be larger.

Reflectance vs Angle of Incidence Method

Another method for determining n and k from the Fresnel equations is to combine equations (7) and (8) to give an expression for the reflectivity of either completely polarized light or completely unpolarized light as a function of n, k, and φ. Graphical methods of solving for n and k can then be used. Various charts have been prepared to aid in this graphical solution (6), (7), (8). In the vacuum ultraviolet region of the spectrum, where complete polarization of the light is difficult, charts for unpolarized light are frequently used. One of the simplest charts of this type is that prepared by Ishiguro and Sasaki (6), which is reproduced in Figure 1. This chart was prepared by evaluating with the aid of a computer the 20° and 70° reflectances of a surface for different values of n and k. The set of values (R_{20}, R_{70}) that had the same n value were connected by a family of curves, and points that had the same k values by another family of curves. Then, given a set of values

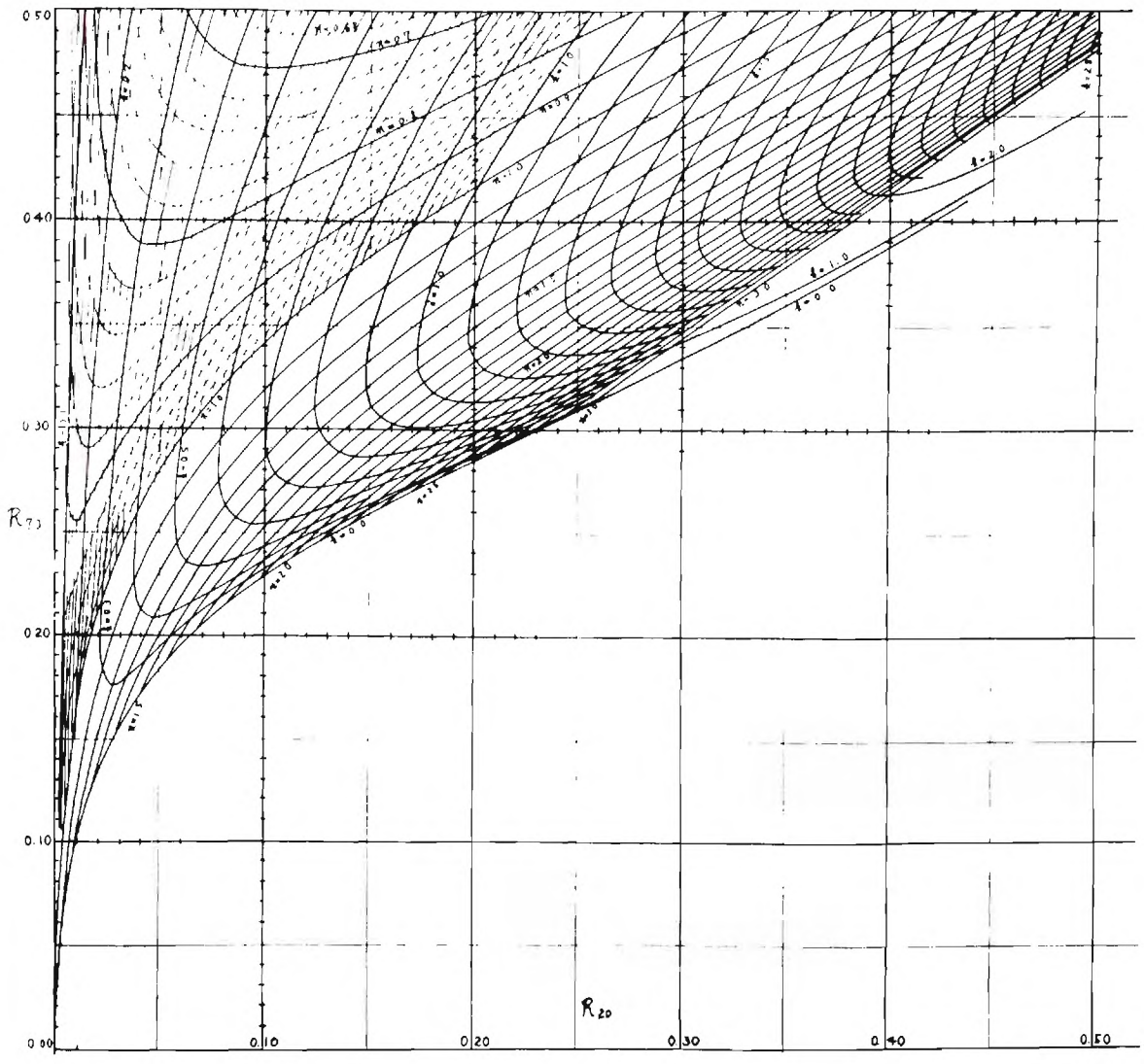

Figure 1. Chart for the Determination of Optical Constants.

(R_{20}, R_{70}) for unpolarized light, n and k can be simply read off the chart. Not only is the light not always unpolarized in the vacuum ultraviolet region of the spectrum, but the state of polarization of the light is usually not even known. Hunter (9) has discussed the effect of polarization of the light on the values of n and k determined by this method.

Thus in order to calculate the optical constants of a material by these reflectance methods, arbitrary extrapolations or approximations of unpolarized light are necessary, and can possibly lead to large errors in the determination of these constants. Of course, optical constants determined from any reflectance measurement are characteristic of the surface of the material, and the presence of any foreign surface layer comparable in thickness to the penetration depth of the radiation could lead to incorrect results by these methods.

Purpose of This Research

Evaluation of Methods of Calculating Optical Constants

The two methods described above are the methods most frequently used for the determination of the optical constants of a material from its reflectivity (8), (10), (11), (12). Both of these methods are inexact, depending on certain approximations or extrapolations. To date no experimental comparison of these two methods has been attempted. A purpose of this research is to calculate the optical constants of a given sample by both methods and to compare the results. To determine which of the two methods gives the most accurate results, the correct values of the optical constants will be calculated at several points by a technique in which experimentally determined curves of reflectance vs angle

of incidence of the light will be curve-fit to the Fresnel equations by adjustment of the parameters n, k, and the polarization of the light.

Determination of the Optical Constants of the Thallium Halides

The thallium halides, although ionic materials, have a much larger dielectric constant than most other ionic crystals, and are therefore similar to semiconductor materials in some of their optical properties. The optical properties of the alkali halides (13), ionic materials with low dielectric constants, and the Group V and IV-VI semiconductors (14), (15), with high dielectric constants, have been extensively investigated. A study of the properties of the thallium halides, on which information is scarce at present, should be a useful contribution to the knowledge of the electronic properties of materials intermediate in their properties between the alkali halides and the semiconductors.

The interpretation of the results for some of the semiconducting materials has been aided greatly by energy band calculations on these materials. For the ionic materials, however, the calculations are incomplete, and no band calculations have been reported for the thallium halides.

The most extensive investigation to date on the optical properties of the thallium halides has been an investigation by Zinngrebe (16) on the absorption spectra of thin evaporated films of TlCl and TlBr, which was limited to the energy range from 3.0 ev to 6.7 ev. This work showed several absorption peaks which were associated with exciton formation and electron transitions in thallium and halide atoms. These peaks, and

the interpretation given them by Zinngrebe, are shown in Table 1. In Table 1 the atomic thallium and halide excitations are shown as reaction equations between the ions and photons producing the excited atomic states. These interpretations were predicted by Zinngrebe on the fact that the energy difference between the second and third peaks in each material corresponds closely to the $^2P_{3/2} - {}^2P_{1/2}$ transition in the halide atom, while the distance between the second and fourth peaks corresponds to the $^2P_{1/2} - {}^2P_{3/2}$ transition in the thallium atom. The distance between the second and fifth peak for TlCl equalled an energy corresponding to the sum of the chlorine and thallium excitation energy. No such peak was found for TlBr.

The temperature dependence of the absorption edge of TlCl at 3.45 ev has been measured by Zinngrebe (16) and Martienssen (17) from 20°K to 600°K, and by Tutihasi (18) from 89° K to 374°K. These investigations yield a strange behavior. Between 200 and 600°K the absorption edge shifts to lower energies with rising temperature, but below 150°K it shifts in the opposite direction. These results can be interpreted as a superposition of two different absorption processes with opposite temperature dependence. At about 200°K the edge of band-to-band transitions coincides with the tail of the exciton band. The former is shifted to lower energy with rising temperatures and then it alone determines the absorption edge of the crystal. But at low temperatures this absorption disappears beyond the tail of the exciton band and only the latter can be observed.

Lefkowitz (19) has studied the exciton structure of TlCl and TlBr by absorption in extremely thin single crystals, and has found absorption peaks corresponding to the $n = 2$ and $n = 3$ exciton energy levels in

Table 1. Low Energy Absorption Peaks in the Thallium Halides (16)

TlCl	TlBr	Interpretation
3.46 ev	3.04 ev	Exciton formation and the beginning of band-to-band transitions
4.95 ev	4.07 ev	$Tl^+ + \left\{\begin{matrix} Cl^- \\ Br^- \end{matrix}\right\} + h\nu \rightarrow Tl + \left\{\begin{matrix} Cl \\ Br \end{matrix}\right\}$
5.05 ev	4.48 ev	$\rightarrow Tl + \left\{\begin{matrix} Cl \\ Br \end{matrix}\right\}^*$
5.82 ev	5.06 ev	$\rightarrow Tl^* + \left\{\begin{matrix} Cl \\ Br \end{matrix}\right\}$
6.02 ev	(5.48 ev)*	$\rightarrow Tl^* + \left\{\begin{matrix} Cl \\ Br \end{matrix}\right\}^*$
$^2P_{3/2} - {}^2P_{1/2}$	for Cl = 0.11 ev	
	for Br = 0.45 ev	
$^2P_{1/2} - {}^2P_{3/2}$	for Tl = 0.96 ev	

*Not found in Reference 16.

TlBr, as well as the large n = 1 peak. Using these peaks in a Mott hydrogenic series (20) of energy levels he has calculated the fundamental absorption band gap of TlBr by assuming the series limit to be at the bottom of the conduction band, and has arrived at a value of 3.115 ev for that band gap. Similar peaks could not be found for TlCl.

Because all of these previous measurements were carried out using thin evaporated films and only covered a limited energy interval, an independent determination of the optical constants of bulk thallium halide single crystals over an extended energy range was deemed to be of interest. Among the thallium halides, only thallium chloride and thallium bromide were obtainable in a stable crystal form at room temperature, and this investigation was confined to these two.

Construction of Equipment

In order to determine the reflectivity of the thallium halides as a function of photon energy, a complete optical monochromator was designed and constructed to cover the desired energy range from 3.0 ev to 21.2 ev. The basic design was similar to that of Johnson (21), but improvements were made in the light source and vacuum system. Since most of the energy range was below 2000 Å (6.2 ev), an evacuated system using reflection-type optics was necessary. A one-meter, normal incidence vacuum ultraviolet monochromator was chosen as the best design. In order to cover such a large energy interval, several light sources had to be selected and modified to fit the monochromator. A McPherson Hinterregger-type glass discharge lamp was chosen to cover the vacuum ultraviolet region. Since windowless operation was necessary

for operation below 11 ev, a high-speed pumping system was assembled for the monochromator. A liquid nitrogen cold trap was necessary to protect the grating and sample from back-streaming of the pump oil. A dc power supply capable of producing high light intensities was designed and constructed for the arc.

A sample chamber was designed in which the reflectivity as a function of angle of incidence of the light on the sample could be measured. A Pyrex rod with a sodium salicylate phosphor coating was used as a rotatable light-pipe and a photomultiplier tube detector was chosen to give the best signal-to-noise ratio for the light emitted from the phosphor.

CHAPTER II

EXPERIMENTAL PROCEDURE

Instrumentation

Monochromator

In a monochromator for the extreme ultraviolet optical region (from 300 Å to 2000 Å), the optical path needed to be evacuated because of the strong atmospheric absorption of light with wavelength below 2000 Å. Also, there could be no lenses or windows in the light path, because the use of transmission optics was not feasible below 1100 Å. The dispersing element of the monochromator should be a reflection-type grating, and should serve to focus the light as well. This requirement was met by having the grating grooves ruled on a concave reflecting surface which, along with the evacuated tube in which it was placed, formed the basis of the monochromator.

Figure 2 shows a diagram of the complete instrument. The main chamber was constructed from a stainless steel tube 8 3/4" in outside diameter with a wall thickness of 1/4". One-quarter inch thick flanges were welded to the ends of the tube, giving a total length of 3 1/2 feet. The tube was mounted on a movable table. One-half inch thick stainless steel end plates for mounting the grating holder at one end of the tube and the entrance and exit slits at the other were vacuum sealed by "O-Rings" to the flanges by means of sixteen 3/8" bolts.

The grating holder was of aluminum and bolted directly to the end

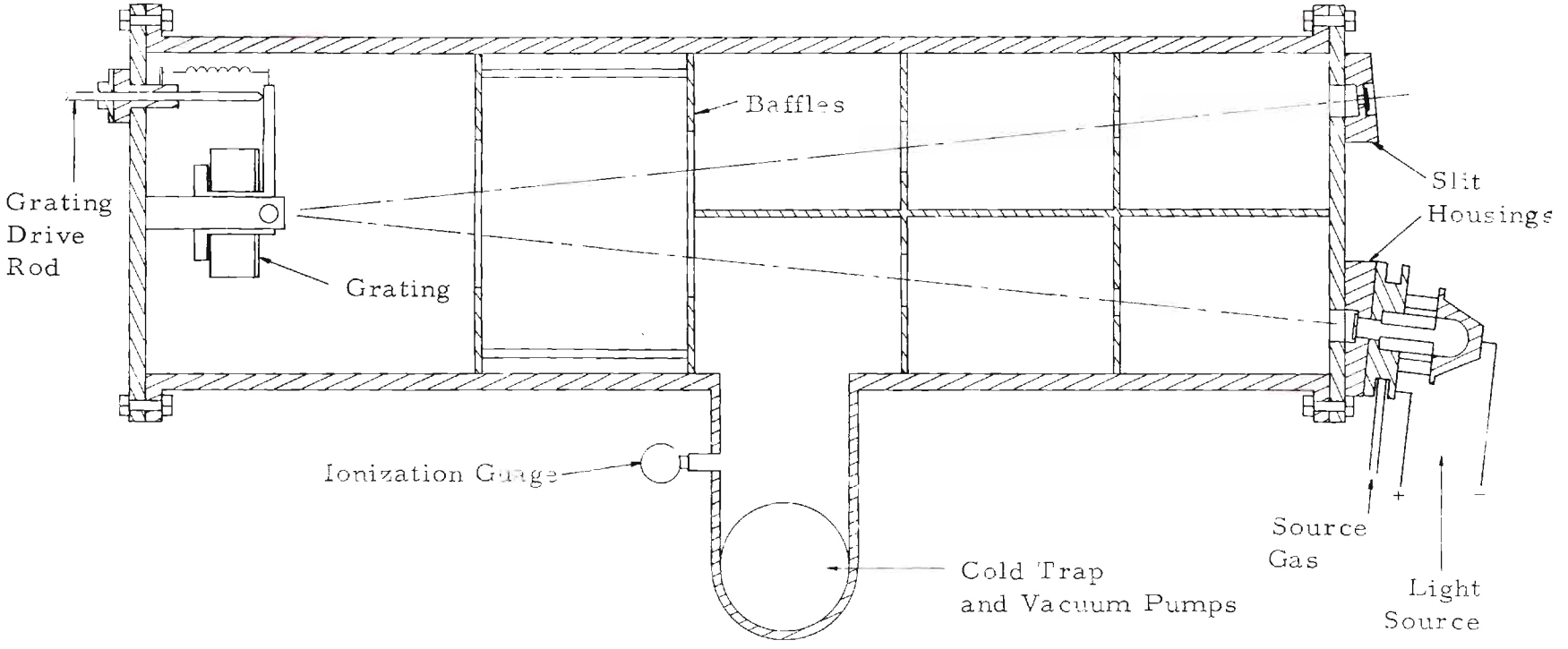

Figure 2. Diagram of the Monochromator.

plate. The grating blank, a 4 1/2" diameter and 1 1/2" thick glass disc, was held in place by a pressure plate, and could be rotated in the holder to align the grooves with the slits. The grating was also adjustable about a horizontal axis for precise alignment, and focusing was accomplished by adjusting the grating-to-slit distance by means of shim brass strips under the mounting.

Four baffles of 1/16" brass sheet were equally spaced inside the chamber to decrease at the exit slit the reflected light from the unwanted portions of the spectrum, and especially the reflected white light from the central image. The baffles and the interior of the chamber were painted with flat black vacuum-stable cathode-ray tube coating, and any gaps between the baffles and the chamber walls were sealed with Apiezon "Q" black wax.

The entrance and exit slits were made of 1/32" stainless steel and attached directly to brass slit housings machined from 5" diameter brass bar. The housings were bolted directly to the slit plate, and gave a 6 1/2" separation between the entrance and exit slits. This separation was the maximum allowable by the chamber diameter and gave just enough room for the attachment of the lamp and sample chamber, which were bolted directly to the slit housings. The slit housings were beveled at an angle of 4° 35' to point the axis of the discharge tube directly at the center of the grating.

The complete system was evacuated through a 1 1/2" pumping line. A Distillation Products Model MC-275 4" water-cooled oil diffusion pump with a capacity of 275 liters per second backed by a high-capacity Welch Model 1397B two-stage mechanical forepump with a speed of 425 liters

per second evacuated the system. A water-cooled baffle and a two quart liquid nitrogen cold trap were located between the diffusion pump and the main chamber. The diffusion pump was never operated without liquid nitrogen in the trap to prevent back-streaming of pump oil which might have contaminated the grating or the sample.

Tank pressure was determined by means of a Veeco CV-1M thermocouple gauge for pressures down to 1 μ, and a Veeco RG-75K ionization gauge tube for pressures below 1 μ. The pumping system was capable of maintaining a tank pressure of 0.2 μ with the forepump alone, or 1×10^{-6} mm with the diffusion pump.

The grating chosen for the monochromator was a Bausch and Lomb replica grating with a one meter radius of curvature. The ruled section was 96 mm by 56 mm with the grooves ruled in three sections on an aluminum surface evaporated on the concave glass blank. The ruling was done in three sections in order to aid in keeping the grooves straight on the curved surface. The groove spacing was 600 lines per millimeter, and the groove faces were inclined at an angle of 2° 35' to the surface. This angular setting made the angle of incidence of the light on the grating equal to the angle of reflection for the 1500 Å wavelength line in the first order and thus concentrated the reflected light in the vacuum ultraviolet region in the first order of diffraction. The surface was overcoated with a 250 Å layer of magnesium fluoride to prevent oxidation of the aluminum surface and also to give constructive interference in the region of interest, as suggested by Hass (22).

In order to scan the dispersed spectrum past the exit slit, the grating was rotated about an axis passing through the center of the

grating tangent to its surface and parallel to the entrance and exit slits. This rotation was accomplished by advancing a finely-threaded drive rod through the end plate of the monochromator. The rod was spring-loaded against an arm on the grating mount (See Figure 2). The grating had to be rotated through 21° to scan the first order spectrum from 0 Å (the white point) to 6000 Å. The grating was rotated by advancing the drive rod 1 1/4" against a 3 1/8" arm. In order to provide the necessary sensitivity in positioning the diffracted beam at the exit slit, the rod and its vacuum-tight casing were threaded with a pitch of 1/32" per revolution. A dial graduated into divisions of 5/1000 of a revolution was firmly attached to the drive rod by means of a pin and slot drive. This arrangement allowed for a sensitivity of 0.35 Å in setting the wavelength.

Light Source

The light source used in the vacuum ultraviolet region of the spectrum was a McPherson Model 630 Hinterregger-type gas discharge lamp. Its 3/16" diameter glass capillary discharge tube was water-cooled, and the aluminum cathode was air-cooled by a fan in the lamp housing. The lamp could dissipate 1000 watts in continuous operation, or 8000 watts in intermittent operation. The lamp was bolted directly to the entrance slit flange of the monochromator and the stainless-steel slit jaws were used as the anode for the discharge.

The lamp was operated as either a high-voltage, cold-cathode dc discharge in hydrogen or helium, or a repetitive high-voltage condensed spark discharge in helium. Commercial cylinder gas was used without purification, and it was admitted to the arc through 3/16" copper tubing.

The gas pressure was regulated by means of a Granville-Phillips variable leak valve. Since no windows could be used for operation in the extreme ultraviolet, the gas was pumped continuously through the entrance slit into the main chamber of the monochromator. This gas leakage was made as small as possible by sealing the exit barrel of the arc to the entrance slits with an "O-Ring" gasket and restricting the gas flow through the slit to an opening 3/16" long with a width equal to the slit width of .010". The 5/16" "O-Ring" fit over a shoulder on the arc barrel, and the barrel was forced against the exit slit by means of a cam drive on a rod passing through the body of the arc. With this arrangement a pressure of 1 μ could be maintained in the main chamber with a pressure of 3 mm in the arc. Since both hydrogen and helium are fairly transparent to their own radiation, this pressure could be tolerated.

The condensed spark discharge was generated in a McPherson Model 720 Dual Mode Power Supply designed for the Hinterregger arc. A 0.0048 μfd capacitor was charged from the secondary of a 15,000 volt rms transformer. An adjustable air gap between two tapered tungsten rods was connected in parallel with the capacitor, and the capacitor was discharged across the gap when the gap breakdown voltage was reached. This charge then passed through the capillary of the lamp and, with an optimum pressure of 70 mm in the arc, produced the fairly intense Lyman continuum from 600 Å to 1100 Å. The air gap in the power supply was irridiated with a quartz mercury lamp and was continuously swept with a jet of compressed air from a DeVilbiss compressor to improve the stability of the spark. A spark repetition rate of 6.5 kilocycles per second was used.

The Model 720 Power Supply also provided for cold-cathode ac

excitation of the arc from the 15,000 volt transformer, but the current density in the arc with this type of excitation was very much smaller than than required to give useful intensities for the photoelectric detection of the reflected light intensities. For this reason a high-voltage dc power supply was designed and constructed from a high power radio transmitter. A diagram of the power supply is given in Figure 3. This supply could maintain a current of 350 ma through the arc at about 900 volts for the required light intensity.

The dc arc discharge was obtained in helium at an arc pressure of 3 mm to give the 584 Å Helium I resonance line. The lamp was also operated with hydrogen at an arc pressure of 10 mm to give the very intense hydrogen molecular spectrum from 850 Å into the visible. When the hydrogen continuum above 1700 Å was used the intense second order hydrogen line spectrum which occurred in that region was filtered out by a 2 mm thick special ultraviolet transmitting fused quartz plate (G. E. Type 102) located after the exit slit.

The composite spectrum produced by the Hinterregger arc is shown in Figure 4. The weaker hydrogen and helium continuum intensities are multiplied by a factor of 10 in the Figure. An extremely weak region from 5.5 ev to 7.7 ev in the hydrogen continuum is clearly shown.

Reflectometer

The sample chamber was of 5" inside diameter tubing with a wall thickness of 1/2". Since the chamber was bolted directly to the exit slit housing, with no other means of support, it was made of aluminum to decrease the weight. The reflectometer was similar to a design by Smith (23), and is shown in Figure 5. The sample holder was mounted on

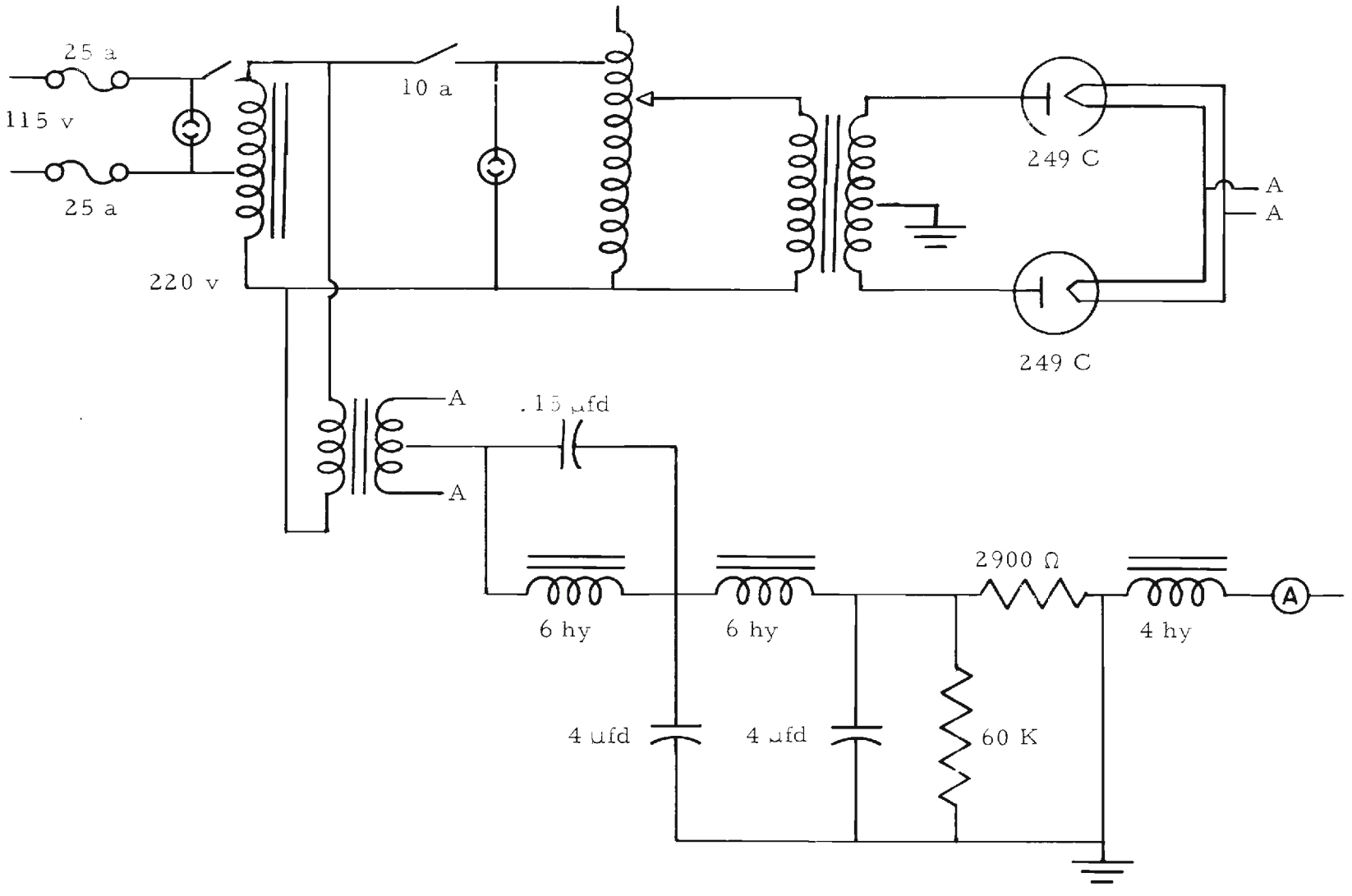

Figure 3. Circuit Diagram of the d. c. Arc Power Supply.

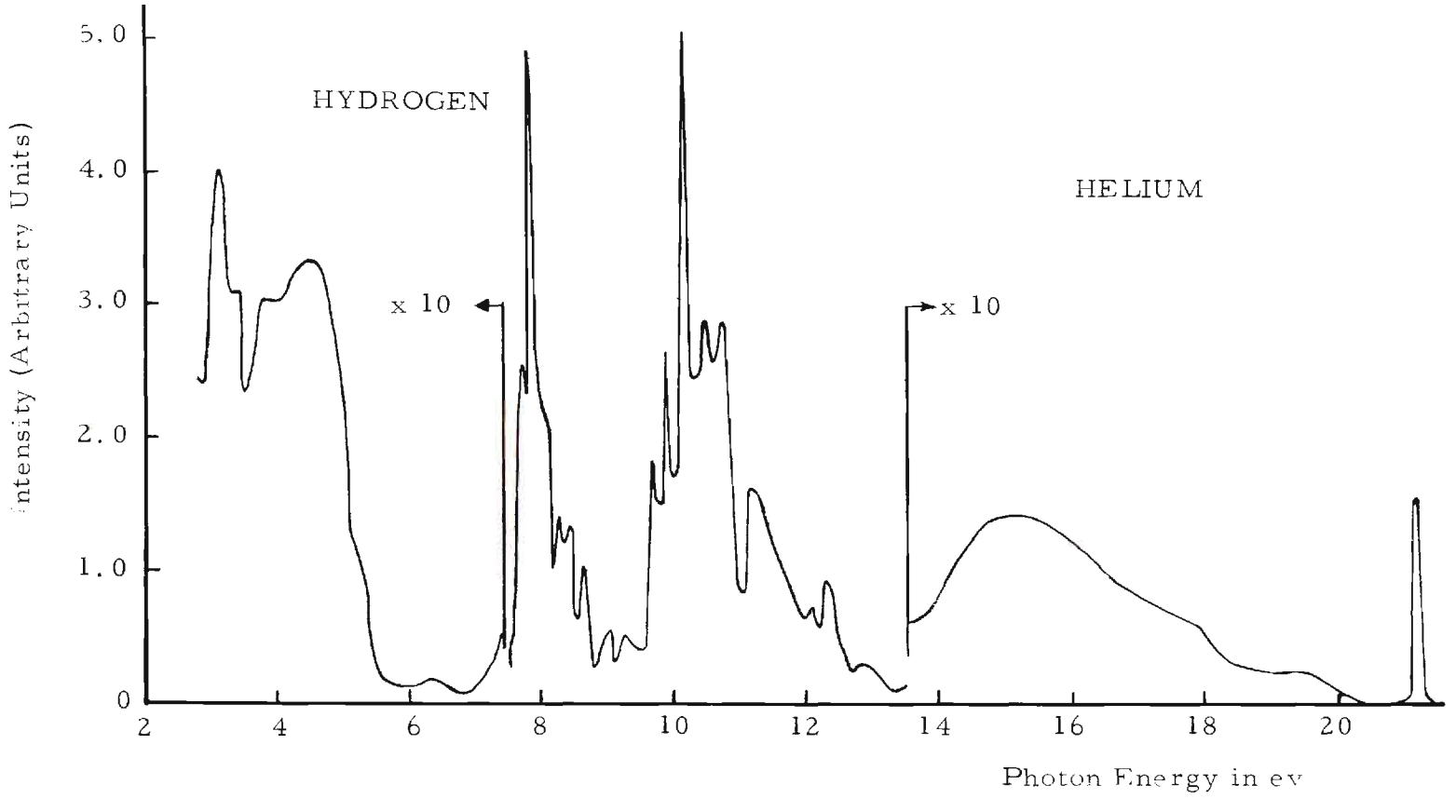

Figure 4. Spectrum Produced by the Light Source.

a 1/4" brass rod in the center of the chamber. It could be rotated completely about its axis or withdrawn from the light beam through an "O-Ring" seal in the floor of the chamber. The angle of incidence of the light on the sample could be set using one quadrant of a 4" radius protractor scale attached to the sample holder rod. With this arrangement the incidence angle could be set to within 0.1°.

The radiation detector was a 3/4" diameter solid Pyrex rod bent as shown in Figure 5. Both ends were polished for the best light transmission, and the rod was coated with aluminum in order to contain that radiation which was incident on the walls at less than the critical angle. The aluminum coating was protected by a layer of Negolac, a nitro-cellulose lacquer. The Pyrex readily transmitted radiation of wavelength above 3500 Å to the photomultiplier tube outside the chamber. For wavelengths below 3500 Å, the entrance end of the detector was coated with a phosphor, sodium salicylate, which was sprayed on the surface in the form of a saturated solution of sodium salicylate in methyl alcohol using a DeVilbiss No. 40 nebulizer, as suggested by Knapp (24). This method gave a very uniform coating whose thickness could be easily controlled. In the presence of ultraviolet radiation, the phosphor fluoresces at approximately 4400 Å (25) a wavelength which was readily transmitted by the Pyrex rod and to which the photomultiplier tube was especially sensitive.

The Pyrex probe was cemented to a 1" brass bushing using Bondmaster M688 adhesive, which formed the vacuum seal. The bushing rotated in an "O-Ring" seal and was bolted to the photo-tube case, within which the photomultiplier tube was mounted to receive the radiation transmitted by the Pyrex rod end-on. This design allowed for the simultaneous rotation

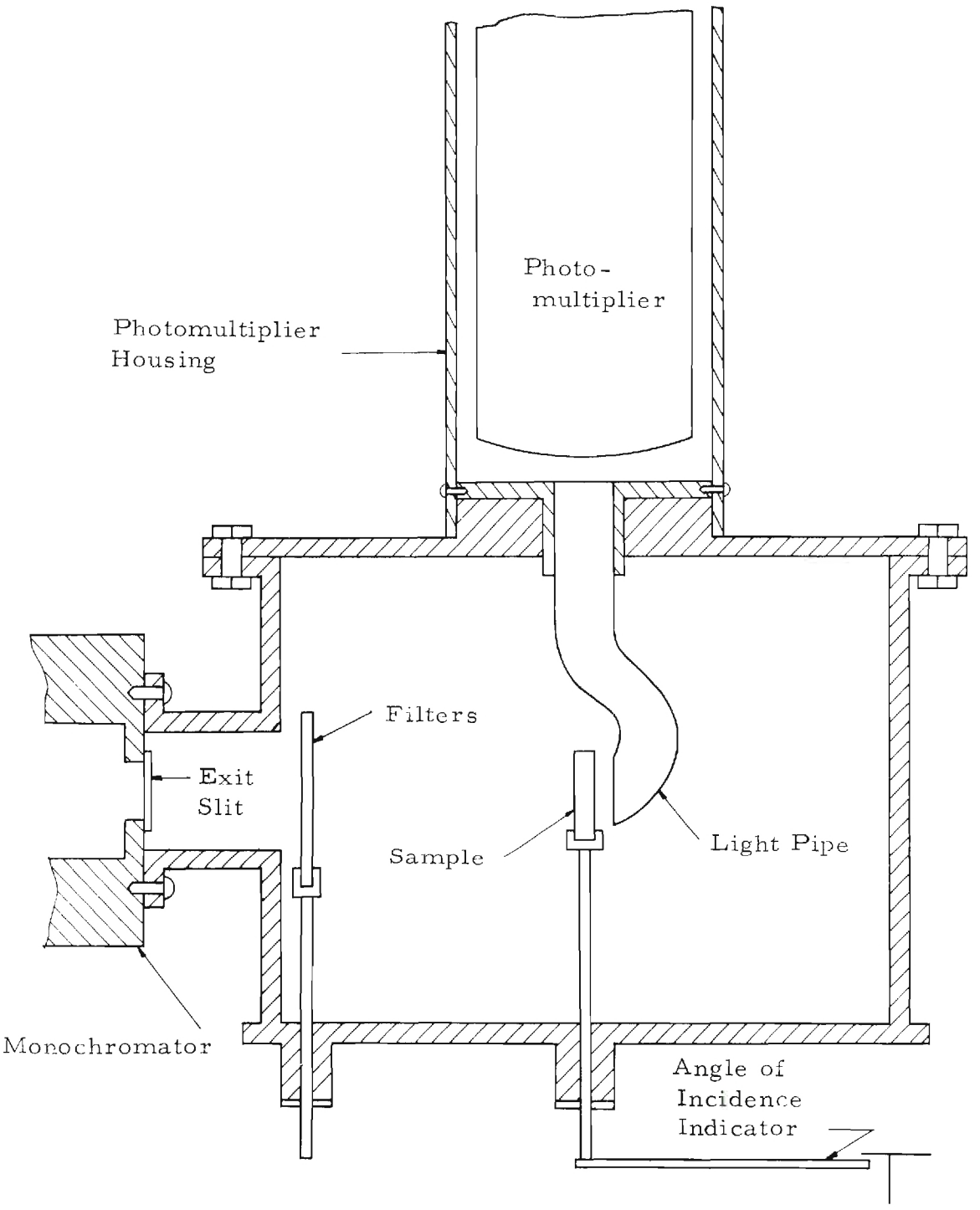

Figure 5. Diagram of the Reflectometer.

of the Pyrex rod and photomultiplier tube and insured that the light would strike the same section of the photocathode at all angles of incidence. There were then no errors due to possible non-uniform sensitivity in the photocathode. Thus the detector was a complete unit with a constant sensitivity for all angles of incidence and all wavelengths.

The Pyrex rod was rotated about a vertical axis through its straight portion coincident with the axis of rotation of the sample. With the reflecting surface of the sample positioned precisely on the axis of rotation, the path length of the light was identical for all angles of incidence and for the incident light. The equal path lengths permitted the determination of absolute reflectivities by taking the ratio of the photomultiplier signals of the incident and reflected light.

The reflectivity could be measured at any angle of incidence between 20° and a maximum value limited by the width of the sample and light beam, which in this work was 70°. The minimum of 20° was determined by the position at which the rod, when intercepting the reflected beam, began to obscure the incident beam.

The photomultiplier tube was either an EMI 9514S or 9607S tube, both of which had an S-11 photocathode. The 9514S gave a slightly better signal-to-noise ratio, but could not be used with the spark discharge source because of electrical interference. For this purpose the 9607S tube was used and the ammeter moved to the grating end of the system. This set-up eliminated most of the interference caused by the spark.

The dynode voltages for the tubes were supplied by an NJE S-326 0-2.5 kv dc power supply. The dynode resistor network was a uniform chain of resistors soldered directly to the pins in the tube base. An

overall dynode voltage of 1500 volts gave the best operating conditions for the tubes, with a dark current of 1×10^{-8} amp. With the 9514S a 0.02" thick brass sheet surrounding the tube was connected to the cathode pin. This was found to be necessary due to a large amount of noise which was present in the tube without it.

The photocurrent was measured by a Keithley Model 415 picoammeter with the 9514S tube or a Model 410 picoammeter with the 9607S. An Esterline-Angus Model AW 6" chart recorder could be used in conjunction with either.

Alignment and Operation of Equipment

The monochromator optical system was aligned by first setting the entrance slit to a 0.010" width and then observing the reflected image of the entrance slit illuminated by a tungsten bulb at the exit slit position. The grating was rotated in the holder to bring the rulings parallel to the entrance slit, as determined by observing the image of the white point and the visible spectrum on a piece of tissue paper taped over the exit slit opening. The instrument was focused by moving the grating holder toward the slits until the white point image was in focus at the exit slit position. The exit slit was then aligned parallel to the white point image and closed to 0.010".

The wavelength dial was calibrated using known spectral lines in the hydrogen and helium extreme ultraviolet region, as well as near ultraviolet and visible lines from a low-pressure quartz mercury arc. The lines used in the extreme ultraviolet were the helium 584 Å and 1640.4 Å lines and the hydrogen 1215.7 Å Lyman-α line. These lines were easy to

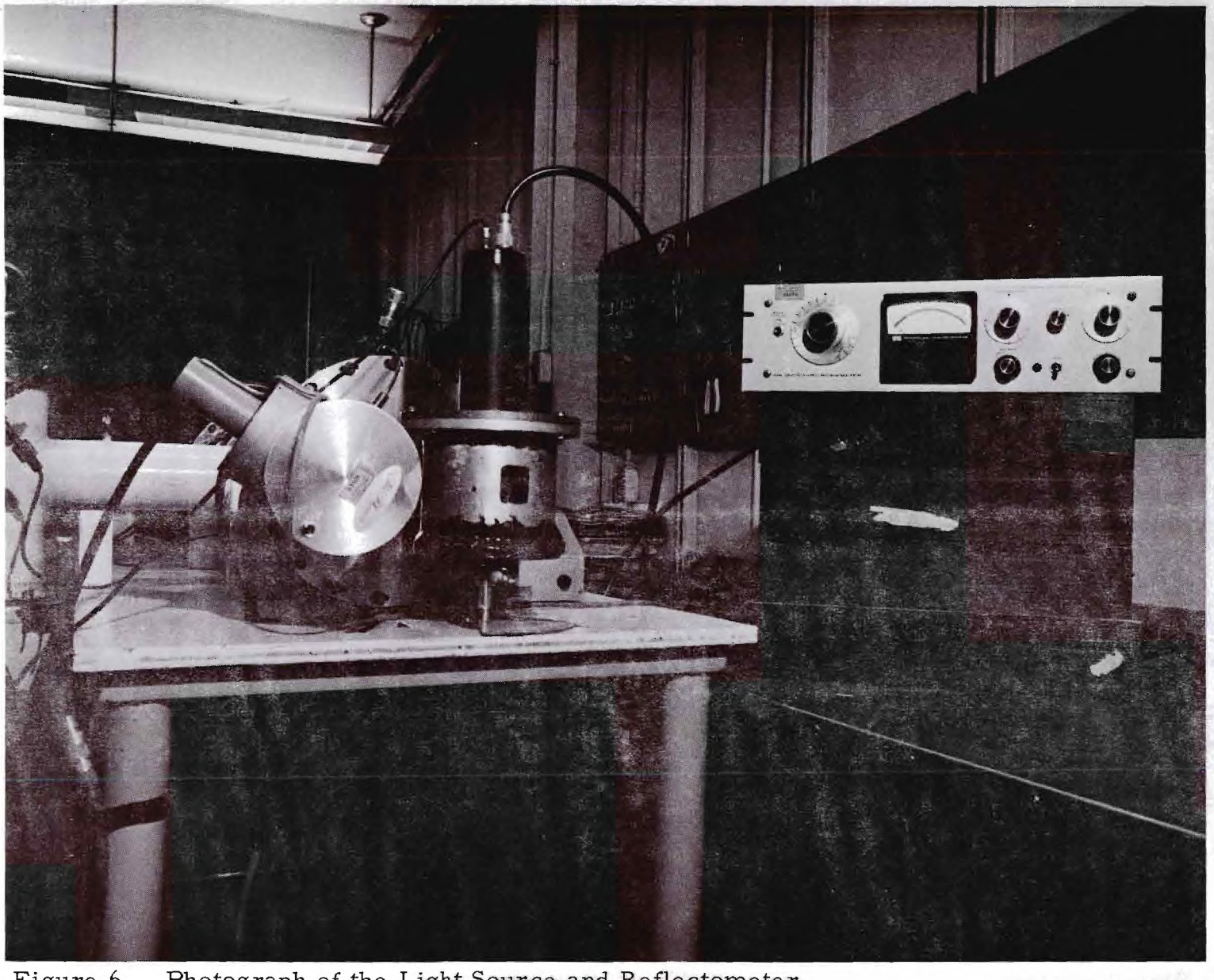

Figure 6. Photograph of the Light Source and Reflectometer.

Figure 7. Photograph of the Monochromator with the Power Supplies.

identify and the wavelengths were known to a high degree of precision. The dial setting corresponding to each calibration line was determined, and the dial setting versus wavelength was plotted. These points fit a straight line relationship to a very good approximation. This linear relationship between dial setting and wavelength can be seen in the grating equation

$$d \sin \theta = \lambda = d \frac{x}{\ell} = kx \ , \qquad (16)$$

where $\frac{x}{\ell} \simeq \theta \simeq \sin \theta$ when θ is small, as it was for the first-order spectrum. In equation (16), x is the distance the grating drive rod advanced and l is the length of the grating drive arm. The slope of the line was 3.48 Å per division of the grating dial. The points all fit the straight-line approximation to within 5 Å, and since this error included any error in dial setting or dial reading, this was taken to be the accuracy with which the wavelength setting was known.

The resolution of the instrument was determined by noting the closest spectral lines that could just be resolved. The monochromator could resolve two lines 7 Å apart at about 1225 Å. This upper limit on the resolution corresponded to an energy resolution of 0.02 ev at 1200 Å, and 0.5 ev at 600 Å.

The state of polarization of the light emergent from the exit slit was determined in the region 3000 Å to 1000 Å (26) using an 8 plate LiF pile-of-plates polarizer, manufactured by the Harshaw Chemical Co. and kindly furnished by Dr. E. T. Arakawa of the Health Physics Branch of the Oak Ridge National Laboratories. The polarizer consisted of 8 cleaved LiF plates mounted in a rotatable cylinder with an aperture of

9/16" diameter. The apparatus was mounted in a brass vacuum-tight cylinder and was driven by a gear arrangement and drive rod passing through an "O-Ring" seal in the housing. A 0-360° scale was mounted on the drive rod to determine the orientation of the plane of incidence of the LiF plates.

The polarizer was mounted directly after the monochromator exit slit and aligned with the light beam using visible light. An EMI 6255B photomultiplier and sodium salicylate phosphor determined the intensity of the transmitted light. To determine the state of polarization of the light in the exit beam, a reading was taken of the intensity transmitted by the polarizer at a given wavelength with the plane of incidence of the LiF plates parallel to the slits and with the plane of incidence perpendicular to the slits. The polarization produced by the polarizer had been determined by Dr. Arakawa, and was given as a function of wavelength by the ratio $\rho = t_p/t_s$, where t_p and t_s were the transmission of the polarizer for light polarized parallel and perpendicular to the plane of incidence of the LiF plates, respectively. The polarization produced by the monochromator, given by the ratio $\rho_m = I_{os}/I_{op}$, with I_{os} and I_{op} the intensities of the components of the partially polarized light emergent from the exit slit, was calculated in the following manner:

$$I_{0°} = t_p I_{op} + t_s I_{os} = t_s \left(\frac{t_p}{t_s} I_{op} + I_{os}\right)$$

$$I_{90°} = t_s I_{op} + t_p I_{os} = t_s \left(I_{op} + \frac{t_p}{t_s} I_{os}\right)$$

$$\frac{I_{0°}}{I_{90°}} = S = \frac{\rho\, I_{op} + I_{os}}{I_{op} + \rho\, I_{os}} = \frac{I_{op}(\rho + \rho_m)}{I_{op}(1 + \rho\rho_m)}$$

$$\rho_m = \frac{\rho - S}{\rho S - 1}\ , \qquad (17)$$

where S was the ratio of the photomultiplier signal when the plane of incidence of the LiF plates was parallel to the exit slit ($I_{0°}$) to that when the plane of incidence was perpendicular to the slit ($I_{90°}$). ρ_m was calculated at intervals of 20 Å from 2000 Å to 1100 Å, the limit of the transmission of the polarizer. The results are shown as a solid line in Figure 8, in which a value of 1.00 for ρ_m indicates unpolarized light. The maximum per cent polarization produced, given by the ratio $\frac{I_{op} - I_{os}}{I_{op} + I_{os}}$, was 14 per cent.

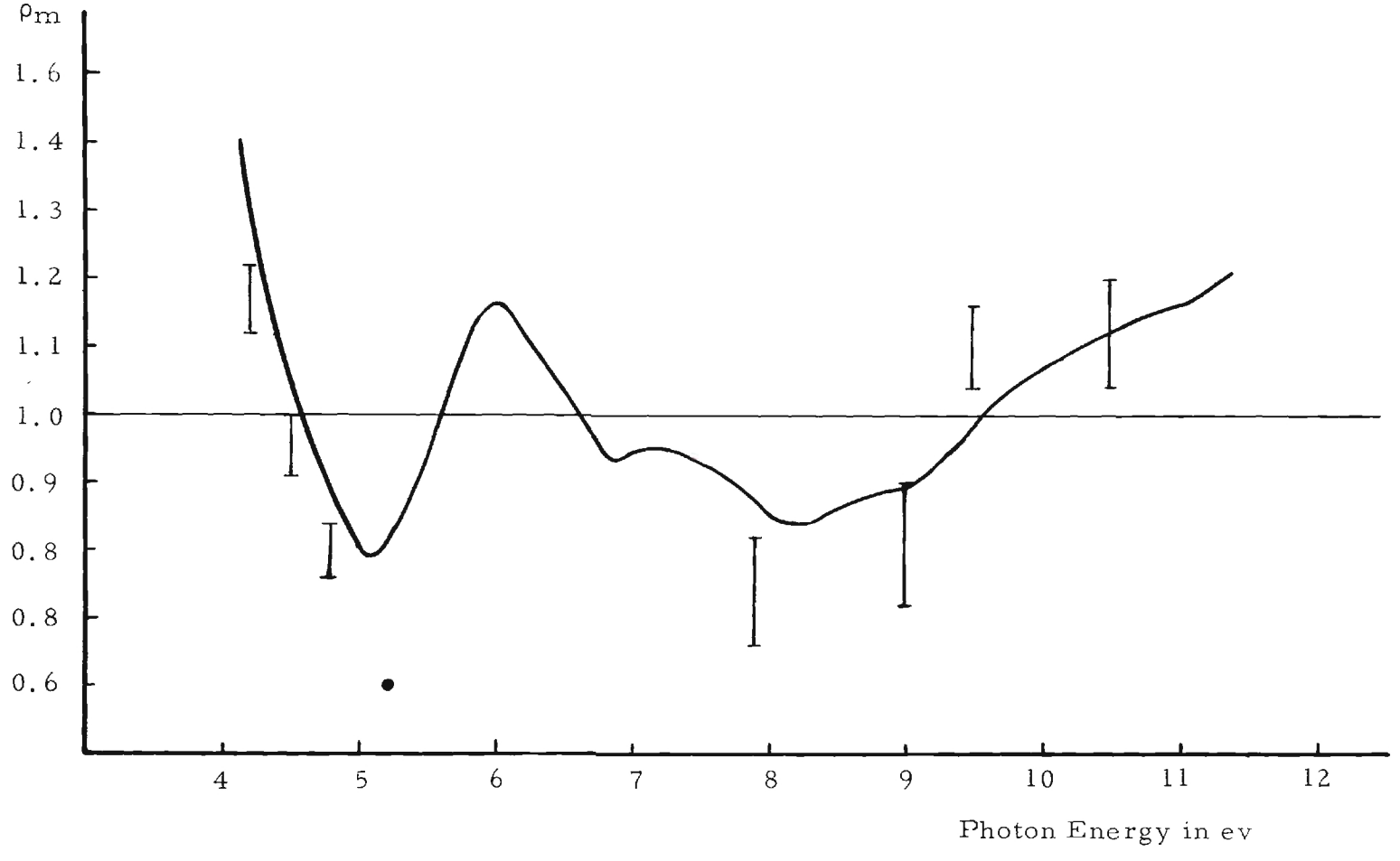

Figure 8. State of Polarization of Light ρ_m from the Monochromator as a Function of Photon Energy.

CHAPTER III

RESULTS

Reflectivity Measurements

Reflection measurements were made on samples of TlBr and TlCl received from the Harshaw Chemical Company, Elyria, Ohio. Two groups of crystals were obtained, one group being 1" x 7/8" x 1/4" with optically polished surfaces, the other group being 7/8" x 7/8" x 1/4" with unpolished surfaces. The unpolished crystals and some of the factory polished crystals were polished using a Westinghouse Mazur lapping and polishing machine. A mixture of methyl alcohol, tincture of green soap, and Fisher "B" alumina was used on a cotton cloth as a polishing compound. Before being polished the samples were annealed for 24 hours at 200°C as suggested by Smakula (27) for the preparation of optical surfaces of the thallium halides.

The polished crystals were aligned in the reflectometer visually using light from the white point and a tungsten bulb. The position for normal incidence of the light on the sample was determined by noting the position of the sample that reflected the beam from the crystal back to the exit slit. This position was used as a basis to fix the angle of incidence of the light on the crystal. The detector position for receiving the reflected beam was then marked for every 5° of incidence angle between 20° and 70°, and it was also marked for receiving the incident beam. The detector position for receiving the incident or reflected beam was not critical, so the only error inherent in the

reflectometer was in setting the incident angle and the zero-point error in the determination of normal incidence, a total possible error of 2°.

Values of the intensities of the incident, 20° reflected, and 70° reflected beams were measured at 0.05 ev intervals from 3 ev to 7.7 ev using the hydrogen continuum. Because both TlCl and TlBr were transparent down to the near ultraviolet, their reflectivities were not determined in the visible, where reflections from the back surface would have complicated the results.

The readings were completed at each wavelength before changing to another wavelength to insure against any errors from long-term drift in the lamp intensity. Corrections were made for scattered light in the incident and reflected beams by setting the wavelength dial to a position at which the lamp, or lamp and filter combination, should have given no output. The scattered light contribution was then taken as the intensity reading at this setting. This reading was always constant down to the white point, so it was assumed to be constant in the region of interest also. The amount of scattered light was always very small, on the order of 1 per cent of the incident intensity, except in the 5.5 to 7.7 ev region, where it was approximately 50 per cent.

Readings were also taken using the line spectrum of hydrogen from 7.7 ev to 13.5 ev at irregular energy intervals depending on the peaks of the lines. These intervals were never more than 0.15 ev. Helium was used in the lamp to determine the reflectivity at intervals of 0.1 ev from 13.6 ev to 20.0 ev, and at the helium resonance line at 21.2 ev.

The reflectivities were determined from several runs on the same sample. At least three, and as much as seven or eight runs for particularly

interesting regions of the spectrum were made, and an average value was chosen for the reflectivity at each point. The values from the different runs on the same crystal agreed to within 1 per cent over most of the range, except for the region from 5.5 ev to 7.7 ev, where the variation was as large as 3 per cent, or the helium region, where variations as large as 5 per cent were found because of the weakness and fluctuations of the lamp in this region. However, these accuracies are acceptable for general reflectance work, and this work showed for the first time the applicability of the helium continuum from the McPherson arc for reflectivity measurements.

Determination of the Optical Constants

The reflectivity curves for TlCl and TlBr as a function of photon energy are shown in Figures 9 and 10. The 20° and 70° reflectivities were used to determine n and k as a function of photon energy using a photographic enlargement of the chart for unpolarized radiation prepared by Ishiguro and Sasaki (6) and shown in Figure 1. In using this chart, the 20° reflectivity was taken as the abcissa of a point and the 70° reflectivity as the ordinate, and the values of n and k were determined from the curves of equal n and k on the chart. The results of this method are shown as dashed lines in Figures 11 through 14. These curves show rather disturbing departures from expected behavior in the low energy region. They indicate a much smaller index of refraction than expected, and also an absorption index that drops sharply to zero at 5.1 ev for TlBr.

In order to calculate the optical constants using a Kramers-Kronig technique, extrapolations were made into the unmeasured low and high

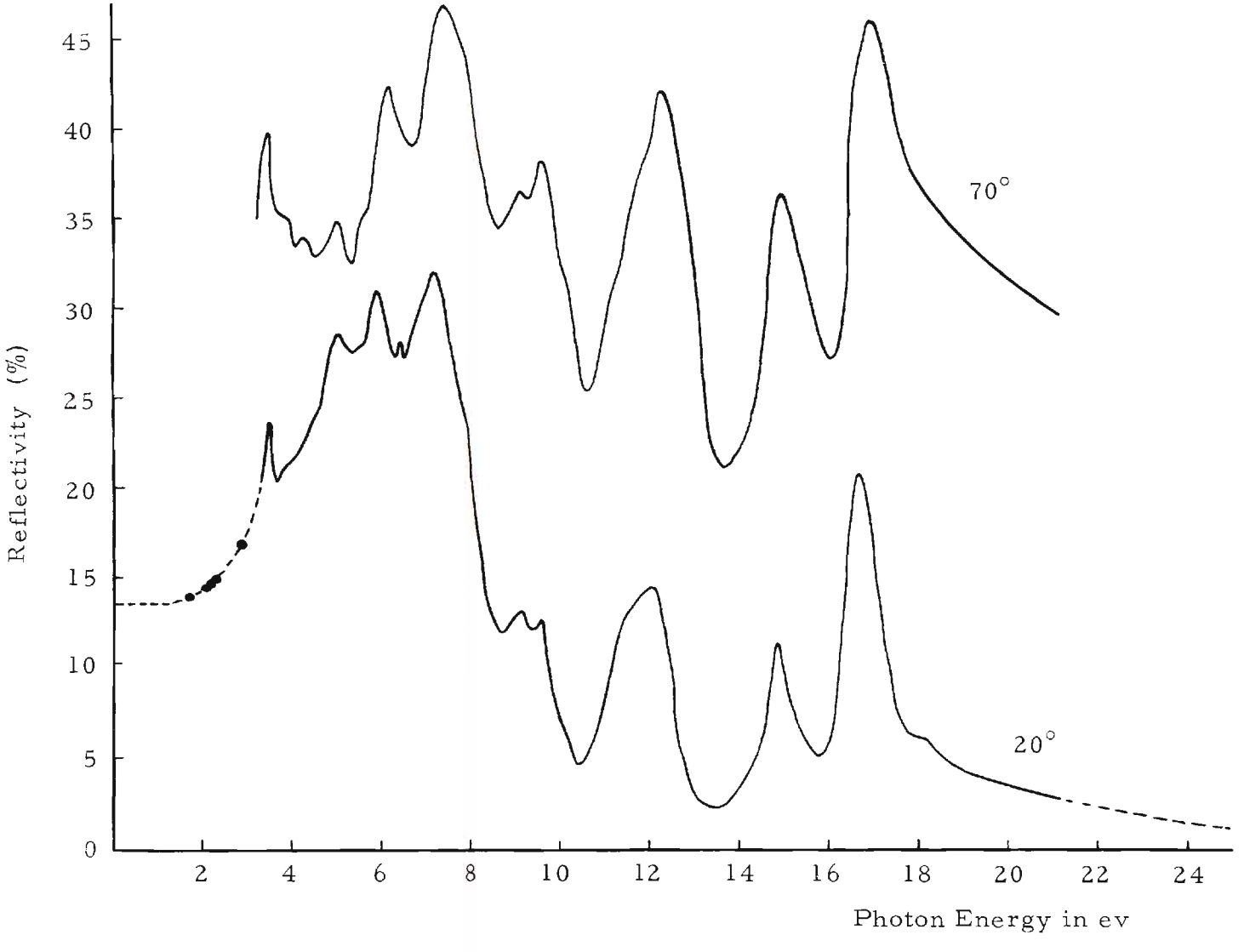

Figure 9. Reflectivity of TlCl vs. Photon Energy.

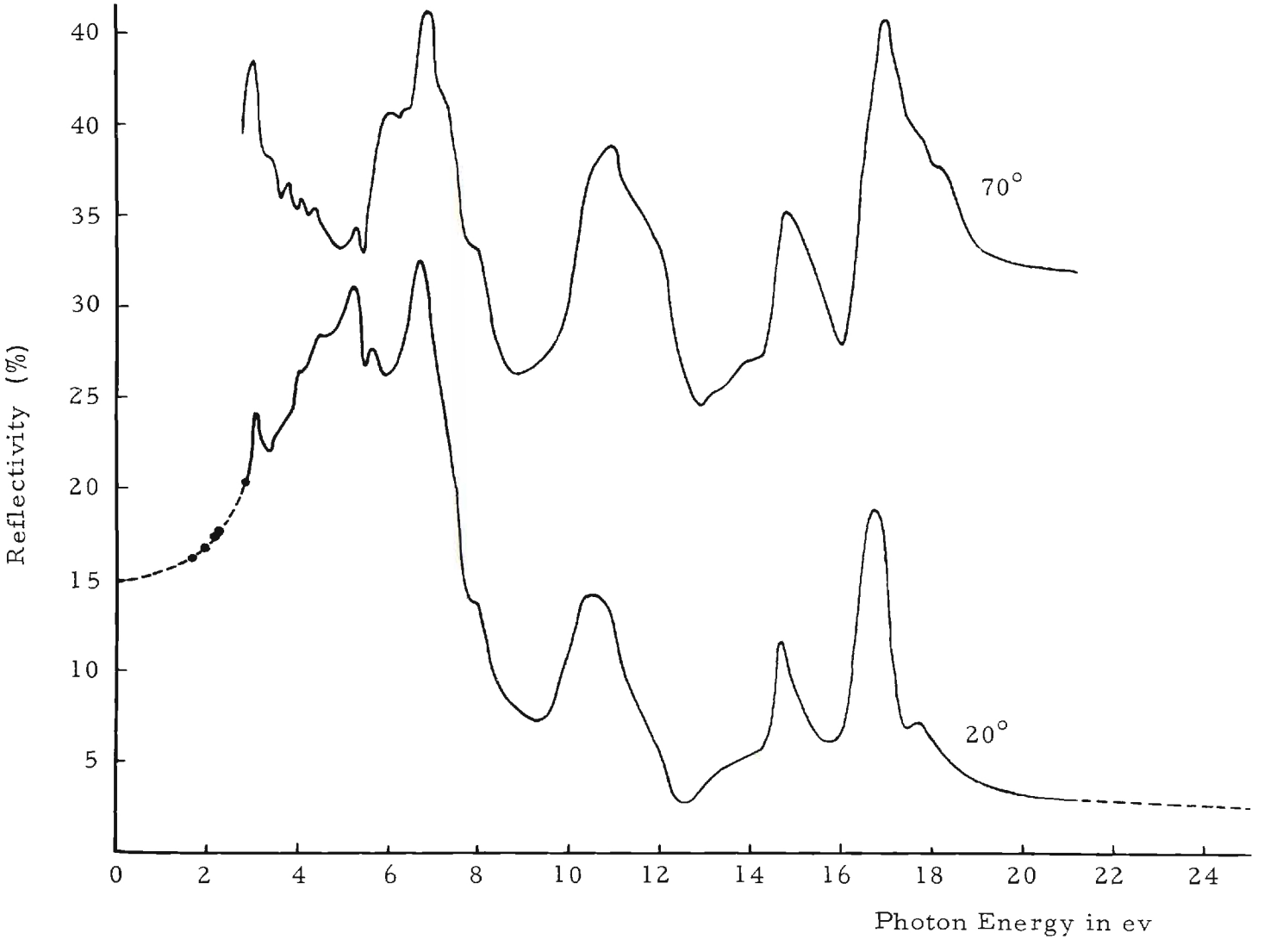

Figure 10. Reflectivity of TlBr vs. Photon Energy.

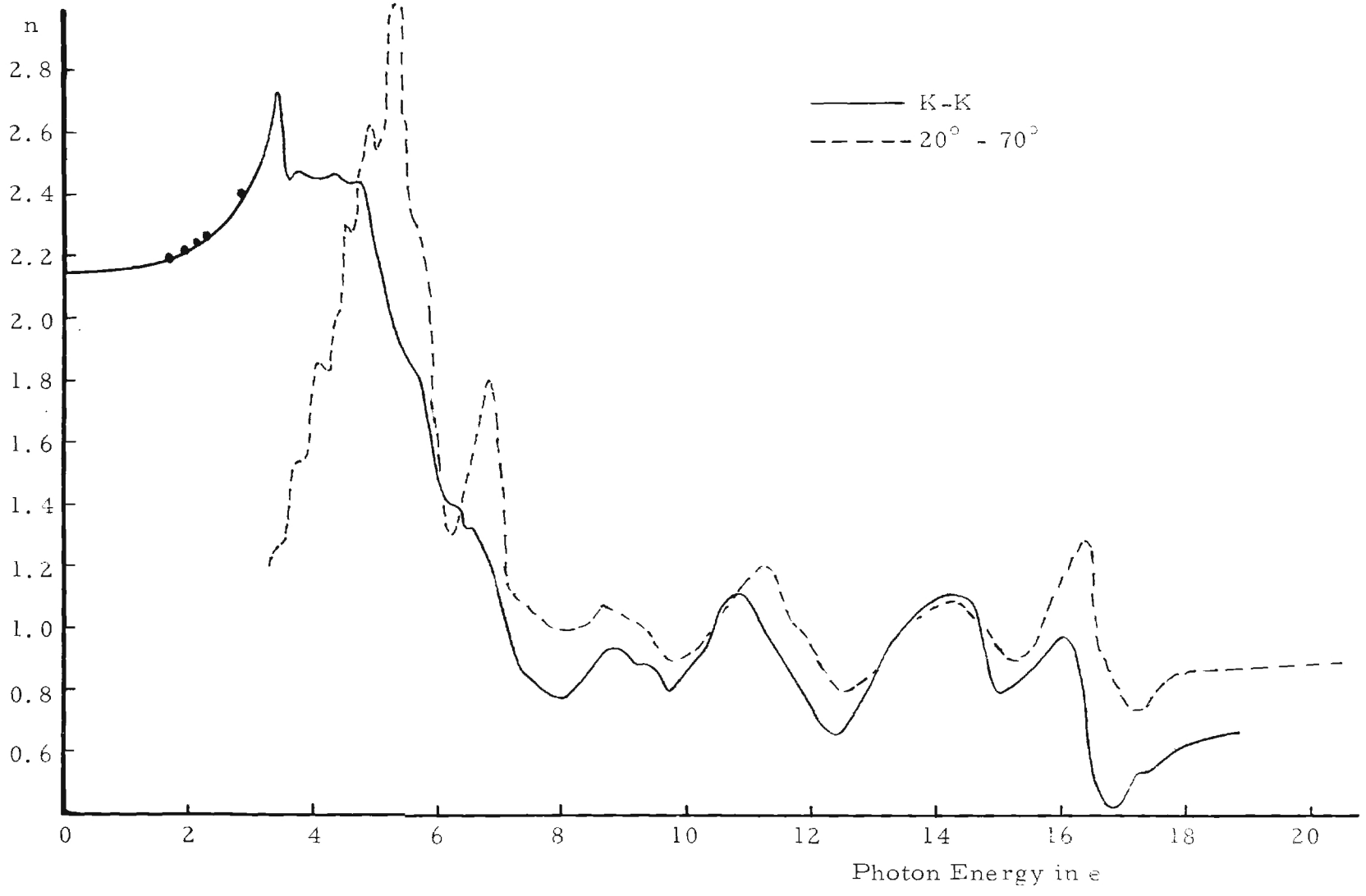

Figure 11. Index of Refraction n of TlCl vs. Photon Energy.

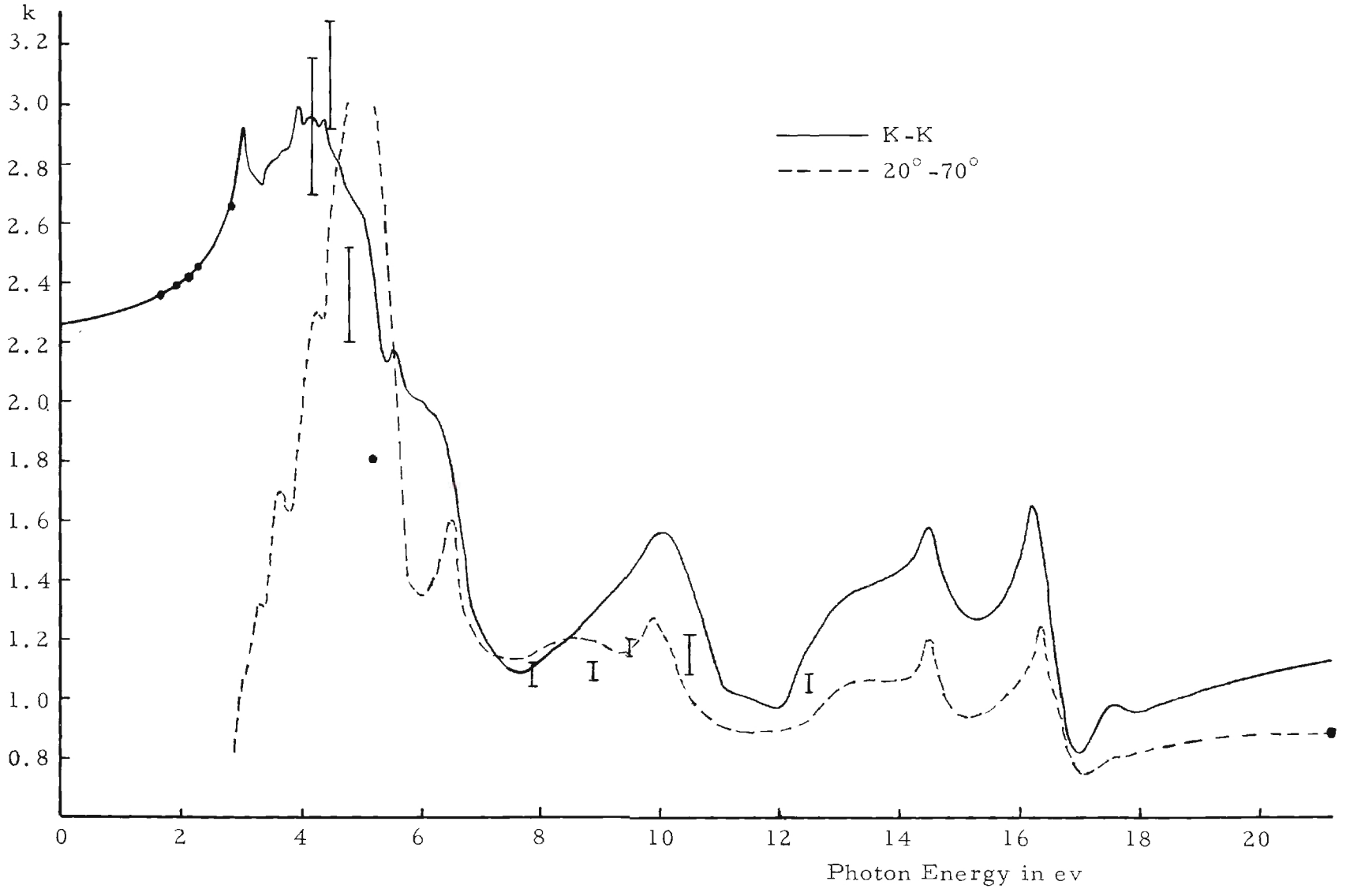

Figure 12. Index of Refraction n of TlBr vs. Photon Energy.

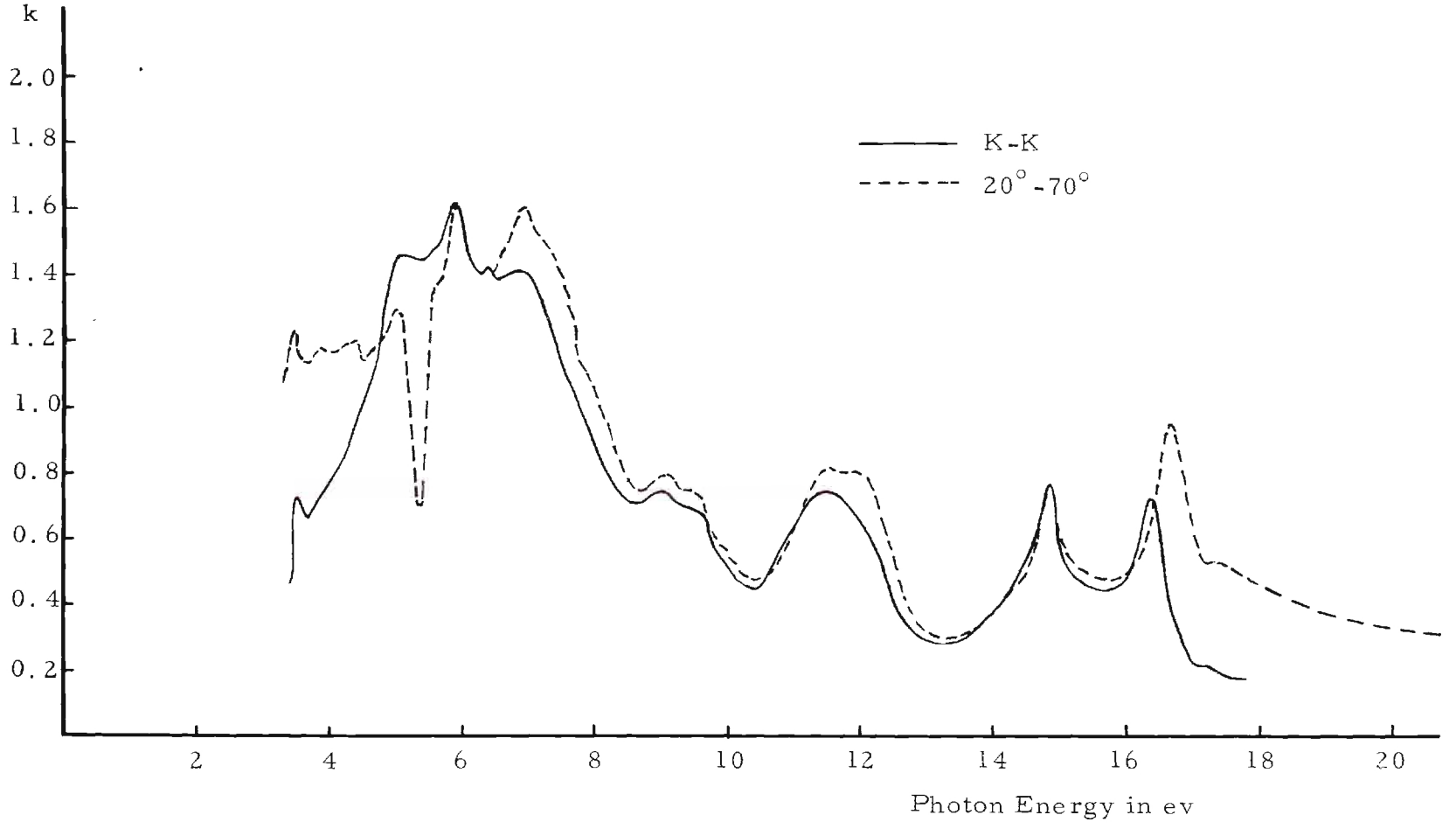

Figure 13. Absorption Index k of TlCl vs. Photon Energy.

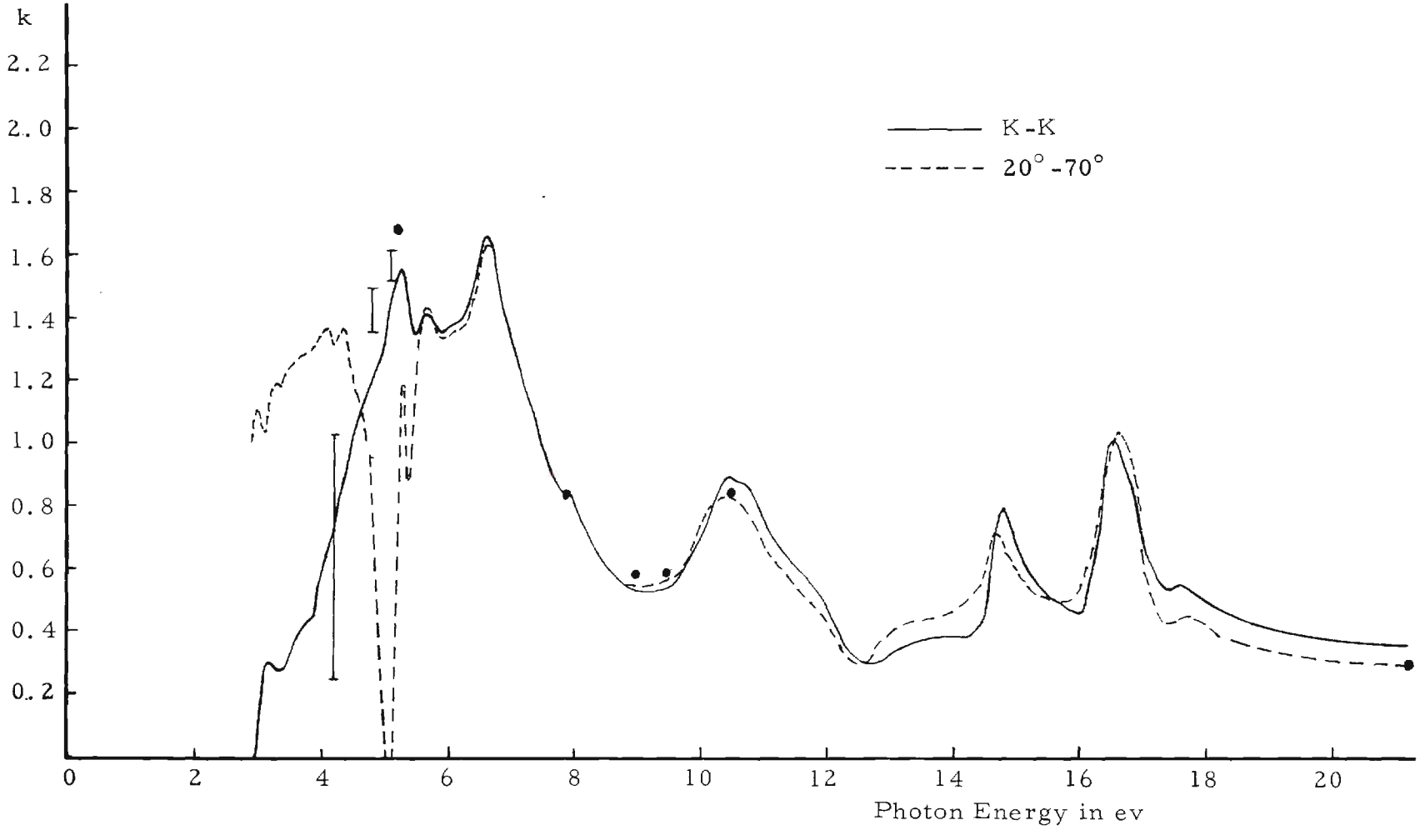

Figure 14. Absorption Index k of TlBr vs. Photon Energy.

energy regions of the spectrum. In the low energy region, where the crystals were transparent, the values of the reflectivity were calculated from the known index of refraction, using

$$R = \left(\frac{n - 1}{n + 1}\right)^2 , \tag{18}$$

the appropriate form of equation (11) when $k = 0$. Values of the index of refraction in the visible region were obtained from the work of Barth (28), and the values of R calculated from these data agreed exactly with the measured values of R in the low energy region. The curve was then smoothly continued with a French curve to zero energy.

The high energy extrapolation was made by fitting the last two measured values of R (20.0 ev and 21.2 ev) to a decaying exponential curve of the form $R(E') = \exp(aE' + b)$. The values of a and b used were:

	TlBr	TlCl
a	$-0.132\ \text{ev}^{-1}$	$-0.1475\ \text{ev}^{-1}$
b	-0.7	-0.415

The value of R at several points up to an arbitrary cut-off point at 100 ev was then calculated from the exponential curve.

The reflectivity data from 0 ev to 100 ev were then put into a computer program. The Georgia Tech Burroughs B-5500 computer was used to evaluate the integral of equation (15) at selected points in the interval from 0 ev to 21.2 ev by means of a trapezoidal approximation. From the value of the phase angle calculated from this integral, n and k were obtained as a function of photon energy (See Appendix B). The

results are shown as solid lines in Figures 11 through 14. These curves are similar to those found with the graphical method in the high-energy region, but give more reasonable results in the low-energy region. Also the values of n calculated by this method agree with those calculated from transmission measurements.

Because of the differences as large as 100 per cent in the values of n and k calculated by these two methods, a measurement of the reflectivity as a function of angle of incidence of the light was made at several selected points for the TlBr sample in order to determine n and k by fitting the experimental curve to the proper Fresnel curve. The sample was not removed from the holder after the 20° and 70° measurements were made, so the same region of the surface of the sample was used, and no errors were possible because of surface differences.

The intensity of the reflected light was measured at intervals of 2.5° from 20° to 70°, the limits of the reflectometer. A correction for scattered light was determined as before, this time for all angles of incidence used. Typical data are shown in Figure 15. The data presented in Figure 15 show that the instrumental polarization of the incident light cannot be neglected, as it gives quite a large change in the high angle of incidence values of the reflectivity from that for unpolarized light.

In order to determine n and k from these curves, a computer program was written to compare the experimentally determined curves to computer-generated Fresnel curves using different values of n, k, and ρ_m, the state of polarization of the incident light (See Appendix B). The correct values of n, k, and ρ_m were chosen by inspection of the RMS deviation between the experimental curve and the Fresnel curve. A

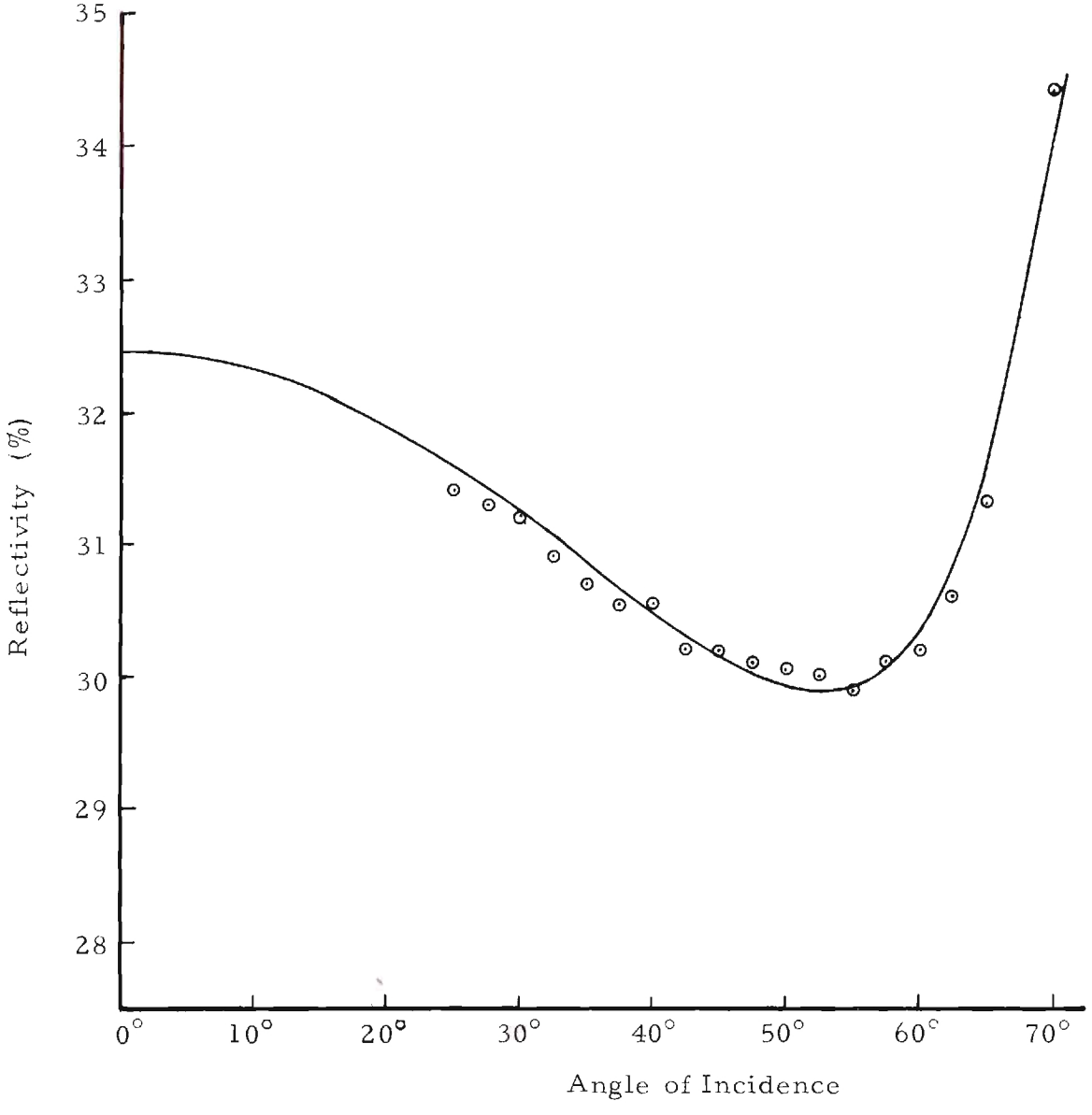

Figure 15. Reflectivity vs. Angle of Incidence of Light for TlBr at 5.2 ev.

range of values, instead of single values of n, k, and ρ_m, gave curves in agreement to within experimental error with the data for some wavelengths. These ranges are shown as vertical lines at the appropriate photon energy in Figure 8, 12, and 14. These results agree fairly well with the values calculated by Kramers-Kronig analysis, but disagree greatly with the results of the graphical analysis in some regions. The polarization of the incident light calculated in this manner agrees well with that determined with the LiF polarizer.

CHAPTER IV

DISCUSSION OF RESULTS

Evaluation of Methods of Calculating Optical Constants

The data presented in Figures 11 through 14 show that the Kramers-Kronig (KK) and graphical (20° - 70°) methods give quite different values for the optical constants in some regions of the optical spectrum. The 20° - 70° results show large deviations from the generally expected results, such as values of n which are very much smaller than the values determined by transmission methods in the transparent region. This method also gives the improbable result that the absorption index k is zero for TlBr at an energy higher than the fundamental absorption band edge (See Figure 14). The 20° - 70° results also disagree at low energies with the values arrived at by the Fresnel curve-fitting method.

The KK results agree exactly with previously determined values of n in the transparent region. Tutihasi (18) used measurements of the transmission to determine the absorption coefficient α as a function of energy between 3.5 ev and 4.5 ev. The absorption index k shown in Figure 13 and determined by KK analysis was used to calculate α. The result agrees in shape as well as in magnitude with the values measured by Tutihasi. The KK values of n and k for both materials agree to within 15 per cent with the values determined from the Fresnel curve-fitting method.

The results for TlCl agree best in the energy interval of 7 ev to 16 ev but begin to diverge past 16 ev. For TlBr both methods give

agreement with the Fresnel curve-fitting method to within 15 per cent over the whole range.

Reference to Figure 8 shows that the regions of large discrepancy in the results of the two methods coincide with the regions in which the light is strongly polarized. This fact suggests that the error in the 20° - 70° method is a direct consequence of the approximation of assuming unpolarized light. At energies for which the light is unpolarized, the curves for the two methods cross. This coincidence is the strongest argument for the assumption that the cause of the disagreement in the two methods is the polarization of the incident light.

Other features of the results can also be explained by considering the polarization of the incident light. The fact that the KK method gives more accurate results can be explained by recognizing that the reflectance for an angle of incidence of 20° is not affected nearly as much by polarization in the incident beam as the 70° reflectance (1 per cent compared to 11 per cent for $n = 2$, $k = 1$, and 15 per cent polarization). Since the KK results depend only on values of the reflectivity for low angles of incidence, and the graphical method depends on values for high angles of incidence, the graphical method will be more in error when polarized light is used.

The computer calculations of Hunter (9) have shown that polarization does not have much effect on the curve of reflectance versus angle of incidence when the values of n and k are small. This result is confirmed by the agreement between the two methods at energies higher than 7 ev, even though the polarization is still large in this region.

The discrepancy in the results of the two methods for energies

higher than 16 ev in TlCl ev in TlCl is probably due to the extrapolation of the reflectivity curve for TlCl used in the KK analysis, since it may be assumed that the 20° - 70° method gives essentially correct results in this region of low n and k. The value of taking data by two different techniques becomes apparent when the results and approximations can be checked for self-consistency.

In considering the Fresnel curve-fitting method of calculating optical constants, the results of Figures 12 and 14 indicate that this method, although giving correct values of the optical constants, is not sensitive enough to use in calculating these constants exactly when n and k are large. In this situation a large range of values of n, k, and the polarization of the light will generate curves that fit experimental points to within a reasonable experimental error. The curve-fitting results of Figure 8 can be used to verify the state of polarization of the light from the exit slit of the monochromator as measured with the LiF polarizer (26). The results previously mentioned are self-consistent.

Discussion of the Optical Properties of the Thallium Halides

As an aid in interpreting the data from this research on the optical properties of the thallium halides, the real and imaginary parts of the complex dielectric constant ε' for TlCl and TlBr were calculated from the values of n and k determined by means of the Kramers-Kronig analysis of the reflectivity data. The relations between ε_1 and ε_2 and the optical constants are

$$\varepsilon_1 = n^2 - k^2 \tag{19}$$

and

$$\varepsilon_2 = 2nk \, . \tag{20}$$

The values of ε_1 and ε_2 for TlCl and TlBr as a function of energy are plotted in Figures 16 and 17. These Figures show several peaks in ε_2 that can be discussed in terms of particular electron transitions in the materials. Note that much of the fine structure in the original reflectivity curves has been obscured in the ε_2 results. Phillips (1) has shown that the integral transform can obscure the fine structure and also result in a shift of the peaks from 0.1 to 0.4 ev.

The steep rise in ε_2 at 3.05 ev for TlBr and 3.45 ev for TlCl has been associated with the fundamental absorption band edge underlying an exciton peak by previous investigators (16), (17), (18). The oscillator-like appearance of the first peak in TlCl at 3.5 ev is consistent with the formation of excitons at this energy. The behavior of the optical constants at an energy associated with an electron transition to a discrete exciton energy level would be expected to be oscillator-like as discussed by Phillips (1). These results cannot be used to ascertain the energy at which band-to-band transitions begin, since the band edge has been assumed to be nearly degenerate with the exciton level and cannot be resolved from it. The band edge of TlCl has been placed at 3.5 ev by Zinngrebe (16) from the results of his investigation of the temperature dependence of the band edge, and at 3.43 ev by Yanagi (29) because of the sharp rise in the photoconductivity at that energy. Either one of these energies for the band edge would not be resolved from the exciton peak in the room temperature data presented here.

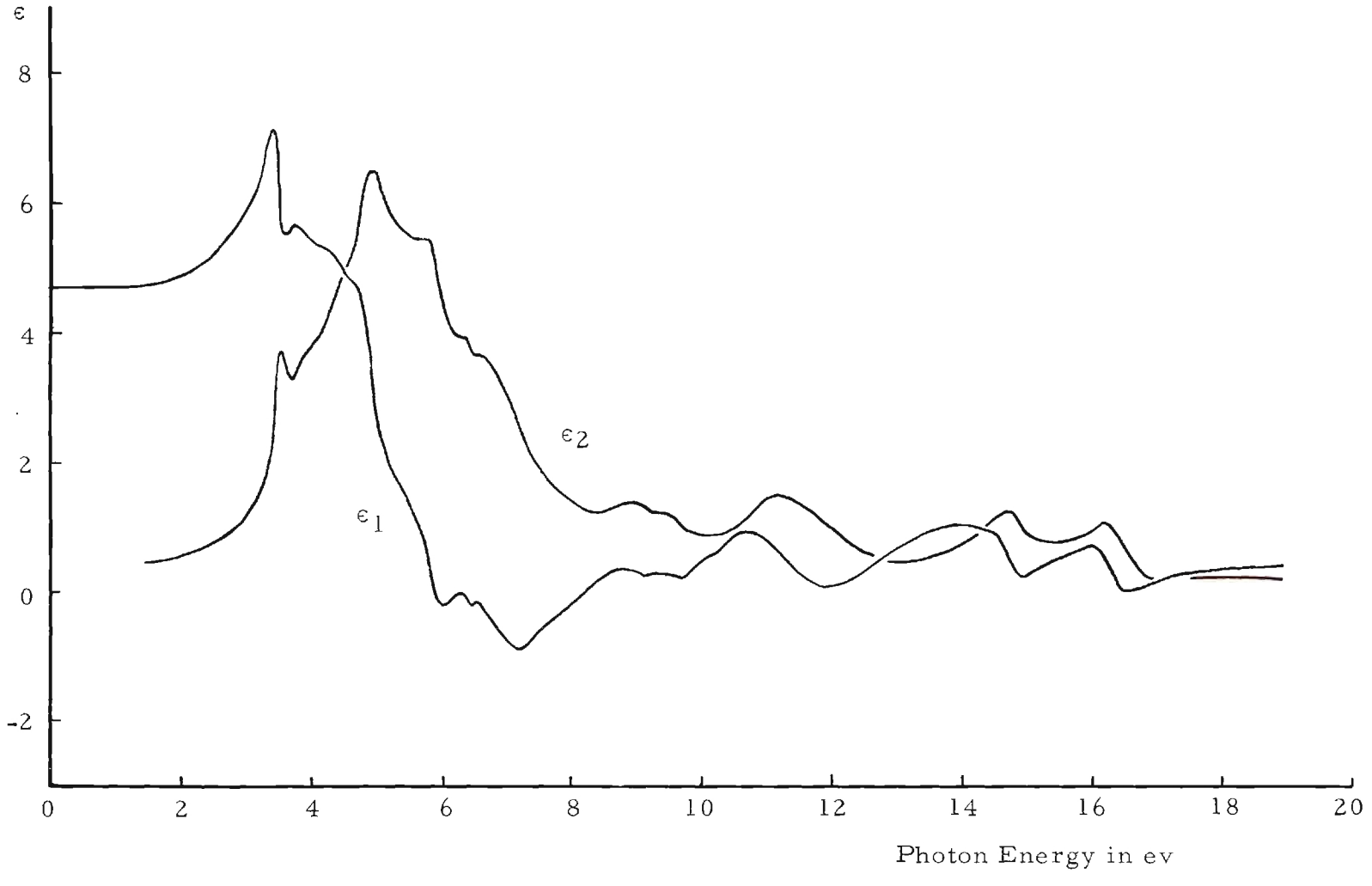

Figure 16. Dielectric Constants ϵ_1, ϵ_2 for TlCl vs. Photon Energy.

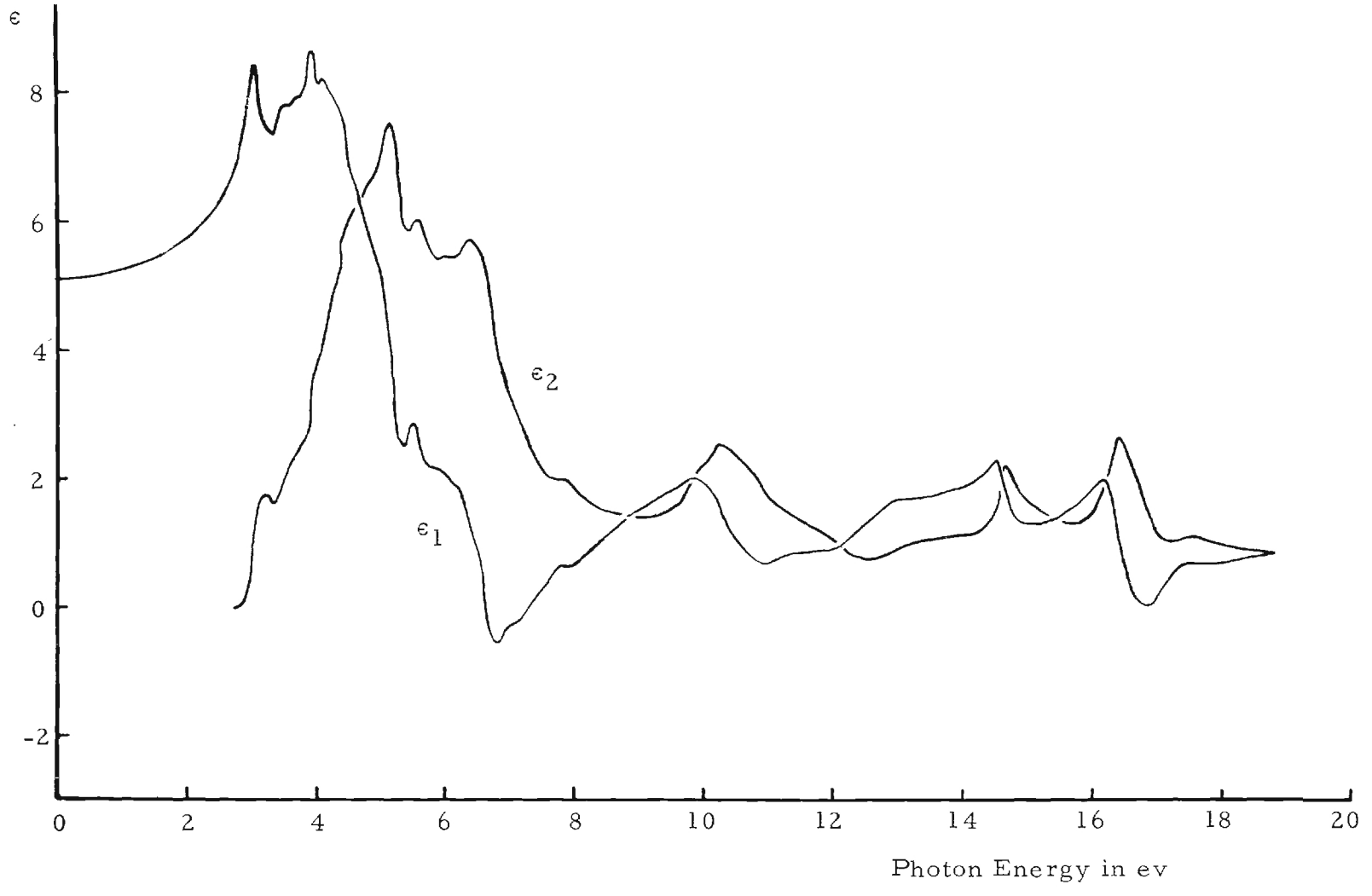

Figure 17. Dielectric Constants ε_1, ε_2 for TlBr vs. Photon Energy.

The absorption edge in TlBr is not oscillator-like in appearance, in contrast with TlCl, but exhibits the behavior calculated by Korovin (2) for transitions between parabolic energy bands, in which ε_2 does not exhibit a peak and ε_1 peaks at an energy corresponding to the band gap. Analyzing the data in Figure 14 for TlBr in the light of these results, the band gap for the onset of band-to-band transitions in TlBr can be placed at 3.05 ev. The exciton peak observed by Lefkowitz (19) is very weak. Lefkowitz has placed the band edge at 3.115 ev by a calculation of the ionization energy of the excitons observed in his work. This assignment agrees with the assignment of 3.05 ev made above within the uncertainty in the present results.

The peaks in TlCl at 4.95 ev, 5.05 ev, 5.82 ev, and 6.02 ev, and in TlBr at 4.07 ev, 4.48 ev, and 5.06 ev, observed by Zinngrebe (16) and associated by him with excited electronic states of the thallium and halide atoms, are observed in the reflectivity data presented in Figures 9 and 10, but appear only as points of inflection in Figures 13, 14, 16, and 17 for the absorption index k and the imaginary part ε_2 of the complex dielectric constant. In addition, the reflectivity and ε_2 for TlBr show a peak at 5.6 ev, corresponding to the excited state of both the thallium and bromine atom, which is missing from the absorption data of Zinngrebe shown in Table 1. The results of this research are consistent with Zinngrebe's interpretation in the low energy region.

The remaining peaks cannot be exactly interpreted without the aid of detailed band calculations. Several general points can be inferred from the present data, however. The rapid decrease in the reflectivity after 7.2 ev for TlCl and 6.7 ev for TlBr is similar to the behavior of

certain metals in the ultraviolet (29), (30). Here the valence electrons are essentially unbound and able to perform collective oscillations. The number of electrons per molecule taking part in these collective oscillations can be calculated from the value of the plasma resonance frequency ω_p associated with these oscillations. This frequency has long been associated (31) with a single large peak in the energy loss function for fast electrons traversing the material. The energy loss function is proportional to the probability that an electron traversing the material will lose a given amount of energy. At an energy equal to $\hbar\omega_p$, the function would be expected to exhibit a maximum. This peak has been observed in conventional energy-loss experiments (32) in which inelastically scattered electrons are energy-analyzed.

The results of energy-loss measurements can also be inferred from optical data (33). The energy loss function is equal to the imaginary part of $\frac{1}{\varepsilon}$, and can thus be calculated from the expression $\varepsilon_2/\varepsilon_1^2 + \varepsilon_2^2$. This expression is plotted as a function of energy for TlCl and TlBr in Figures 18 and 19. Since the values of ε_1 and ε_2 calculated from the Kramers-Kronig analysis are in error beyond 16 ev, the values calculated from graphical analysis are also determined and shown as a dashed line in Figure 19 for TlCl. Peaks appear in these functions in a one-to-one correspondence with peaks in ε_2, though shifted (~0.3 ev) to slightly higher energy. The low energy peaks are small, due to the magnitude of ε_1 and ε_2 in this region. This structure can be associated with interband scattering and is analogous to results obtained for the alkali halides by Phillip and Ehrenreich (13). In addition to these interband scattering peaks, a large broad peak

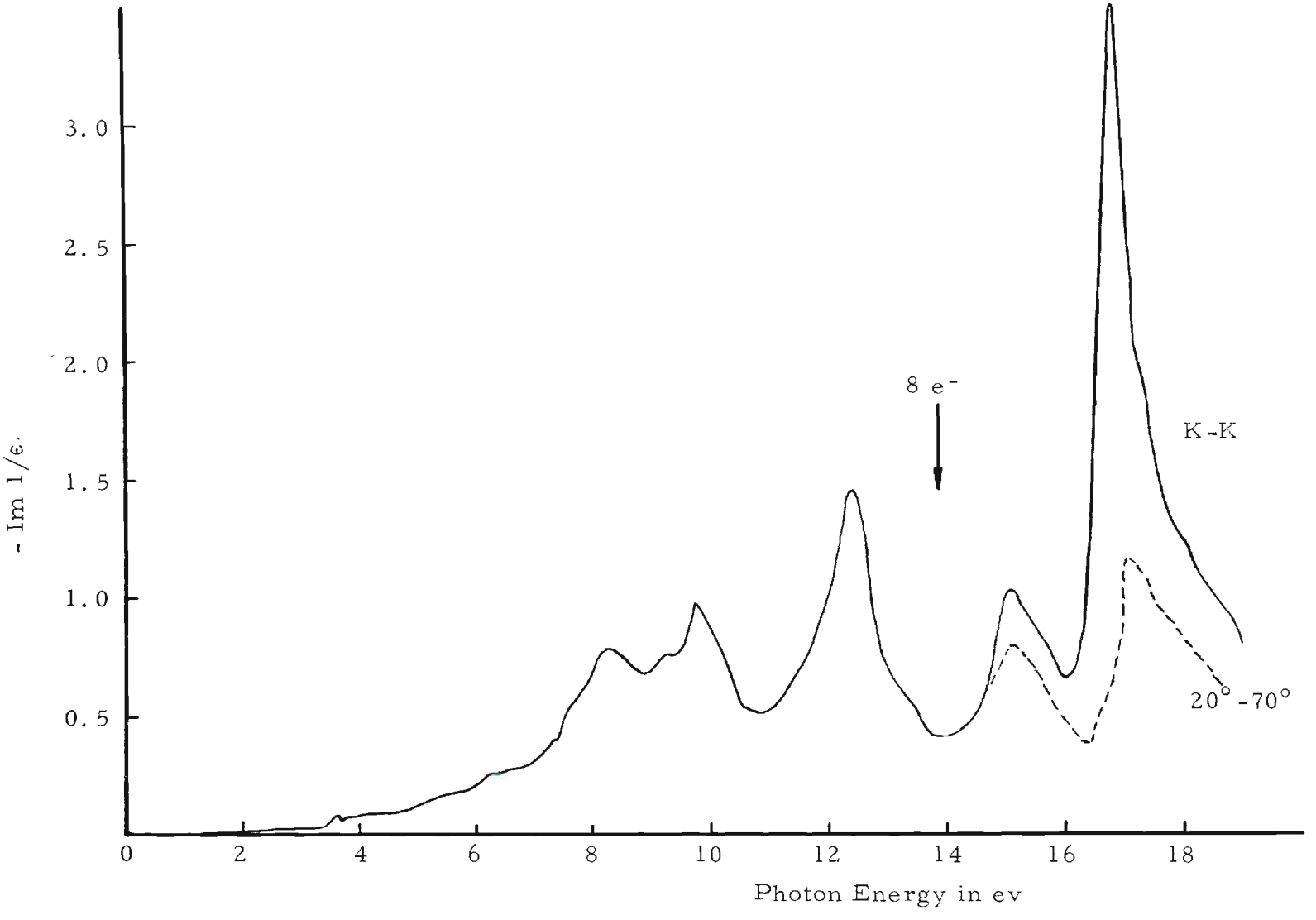

Figure 18. Energy Loss Function - Im 1/ε for TlCl vs. Photon Energy.

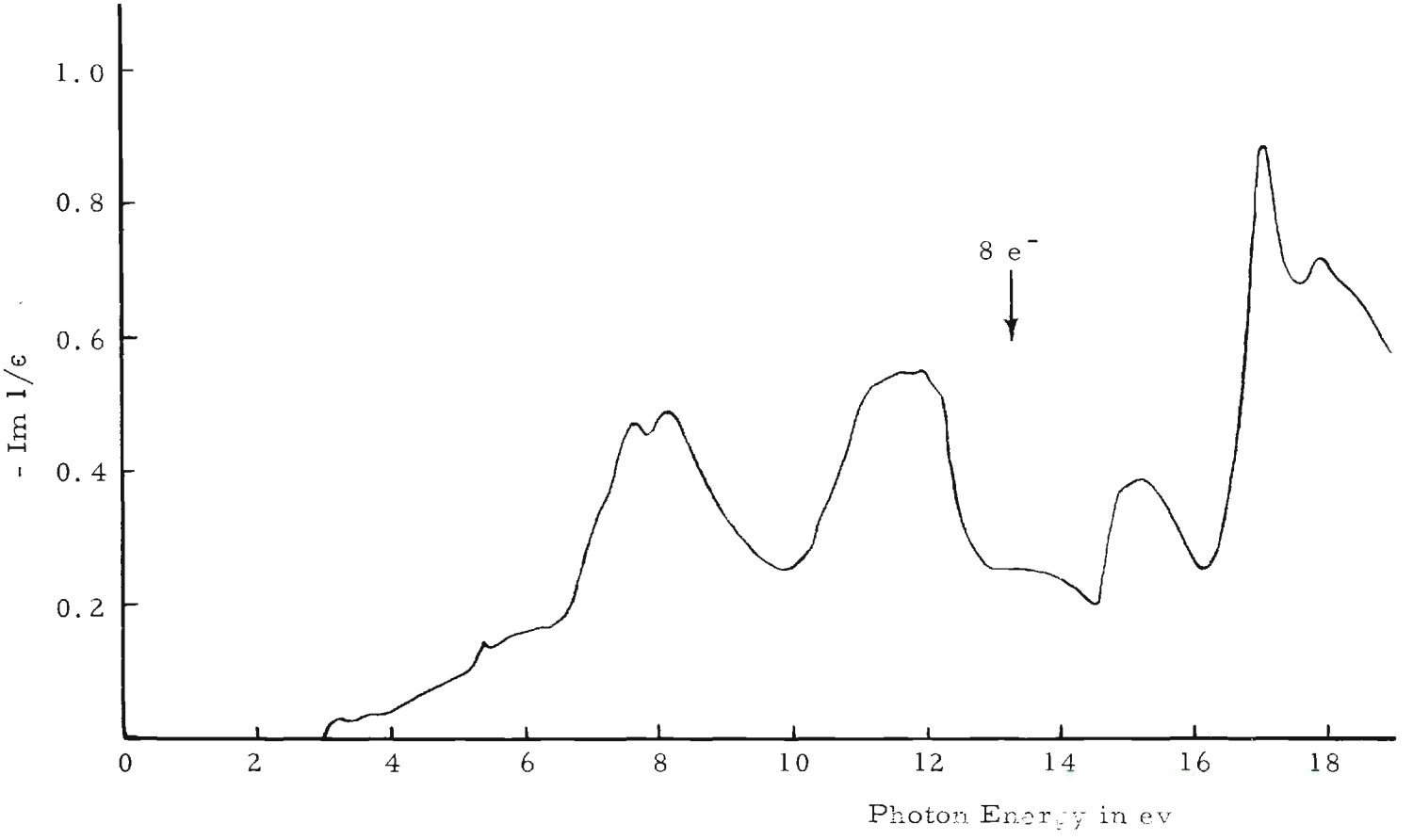

Figure 19. Energy Loss Function -Im $1/\varepsilon$ for TlBr vs. Photon Energy.

appears at 11.8 ev for TlBr and at 12.4 ev for TlCl. This peak is separated by a much larger energy interval (~2 ev) than the interband scattering peaks from any of the peaks in ε_2. Results for the alkali halides are similar but not as pronounced. The work of Phillip and Ehrenreich shows two barely resolved peaks; the lower energy one can be associated with a peak in ε_2, while the higher energy peak has no correspondence with a peak in ε_2. The magnitude of this "extra" peak is ~1.0 and has been ascribed by the authors to the plasma resonance.

In order to locate the corresponding plasma resonance peak for the thallium halides, the density of "free" electrons in the conduction band able to undergo collective oscillations would have to be known. A rough estimate of the energy gaps between the various bands for an ionic material can be derived from a table of atomic energy levels. Table 2 is taken from "Atomic Energy Levels" by Bearden and Burr (34) and shows the energies associated with a particular atomic level in electron volts for chlorine, bromine, and thallium. Only the highest levels are shown. This table indicates that one would expect eight free electrons per molecule at an energy above ~10 ev for both TlBr and TlCl; two electrons from the Tl^+ 6s band, and six electrons from the next lower-lying Br^- 4p band or the Cl^- 3p band. The next lower levels, the halide s-bands, are ~30 ev below the continuum and would not be expected to contribute to optical processed in this region.

The plasma resonance energy $h\omega_p$ can be found (33) from the expression

$$\frac{1}{2}\pi\omega_p^2 = \int_0^\infty \omega\varepsilon_2(\omega)d\omega = \frac{2\pi^2 Ne^2}{m} n \,. \qquad (21)$$

This gives

$$\hbar\omega_p = \frac{4\pi^2 Ne^2}{m} n^{1/2} , \qquad (22)$$

in which N is the molecular density of the crystal in molecules/cc and n is the number of free electrons per molecule. Using a value of eight electrons per molecule for n, the calculated plasma resonance energy is 13.5 ev for TlBr and 13.9 ev for TlCl. If as in the alkali halides the assumption is made that the broad peak in the energy loss function at 11.8 ev for TlBr and 12.4 ev for TlCl consists of a low energy peak associated with the interband transitions at 10.2 ev for TlBr and 11.2 ev for TlCl, and a higher plasma resonance peak unresolved from the interband peak, the calculated values of the plasma resonance energy assuming eight electrons per molecule are in good agreement with the experimental data.

For a finite range of integration, equation (21) can be used to define n_{eff}, an effective number of free electrons contributing to the optical properties in the range up to a given energy:

$$\frac{2\pi^2 Ne^2}{m} n_{eff} = \int_0^{\omega_o} \omega \varepsilon_2(\omega)\, d\omega . \qquad (23)$$

In the absence of bands lower than the p-bands of the halide ion, n_{eff} would be expected to saturate at a value of eight. A plot of n_{eff} as a function of energy from a computer calculation using the Kramers-Kronig values of ε_2 for TlCl and TlBr are shown in Figure 20. For TlCl the graphically determined values of ε_2 were also used above 14 ev the

Table 2. Atomic Energy Levels for Chlorine, Bromine, and Thallium (34)

	Level	Energy (ev)	Number of Electrons per Level in Ion
Chlorine	2s	277	2
	2p (L_{II})	201.6	6
	2p (L_{III})	200.0	
	3s	17.5	2
	3p	6.8	6
Bromine	3p (M_{IV})	70.1	10
	3p (M_V)	69.0	
	4s	27.3	2
	4p (N_{II})	5.2	6
	4p (N_{III})	4.6	
Thallium	5p	75.4	6
	5d (O_{IV})	15.3	10
	5d (O_V)	13.1	
	6s	- 3.2	2

results shown as a dashed line. The curves of Figure 20 indicate that there is considerable contribution from lower lying electron states to the optical properties of these materials only at a fairly high energy. The fact that n_{eff} is less than eight in the region of the plasma resonance indicates that the oscillator strength for valence band excitation is not exhausted in the region of the plasma resonance.

The integral of equation (23) may be considered to be an experimental self-consistency test of the Kramers-Kronig relations connecting ε_1 and ε_2. By contrast, the contribution to n_{eff} from core states is so significant that these plots cannot be used to establish any possible contradiction to the present form of the Kramers-Kronig relations

The last two peaks at 14.7 ev and 16.4 ev are oscillator-like, and can reasonably be associated with atomic transitions in the Tl^+ ion. The association with the thallium ion is based on the evidence that the peaks appear at exactly the same energy for both TlCl and TlBr.

The results of Figures 18 and 20 indicate that great care must be exercised at high energies in interpreting data that depends on a Kramers-Kronig analysis using an extrapolation into the high energy region of the spectrum.

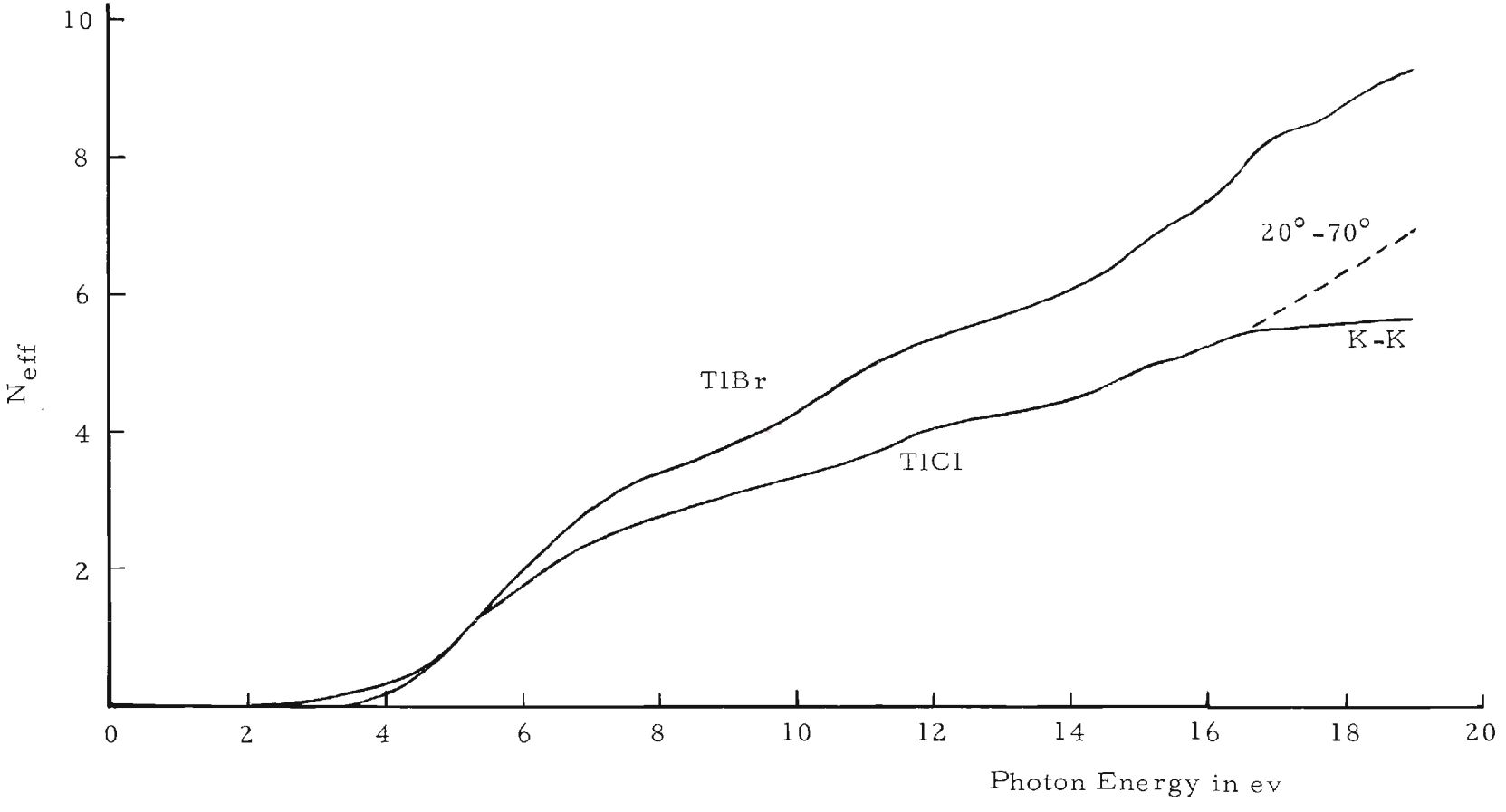

Figure 20. The Effective Number of Electrons N_{eff} Contributing to the Optical Properties of TlCl and TlBr as a Function of Photon Energy.

CHAPTER V

RECOMMENDATIONS FOR FURTHER RESEARCH

Further evaluation of the methods of calculating optical constants from reflectivity data can be carried out using the results of a recent investigation by Roessler (35) on a method of analyzing data by the Kramers-Kronig technique in which an extrapolation beyond the measured region of the spectrum is not necessary. Accurate values of n and k have been calculated in this work at the high energy region of the measured spectrum, where extrapolation errors are greatest in the Kramers-Kronig analysis. Using the reflectance curves from this work, the results of Roessler's method of analysis could be compared to the correct values.

A large amount of work remains to be done on the optical properties of the thallium halides. Of primary importance would be a repeat at lower temperatures of the reflectivity work reported here. The low temperature results would aid in the interpretation of the transitions observed in this work, and facilitate any calculations on the band structure of the thallium halides that might be made in the future. There are optical properties other than the behavior of the optical constants that can further aid in the determination of the electronic properties and energy band structure of these materials. An example is the measurement of the photoconductivity of the materials, which can be used to determine at what energy electron excitations to the conduction band occur.

Results on TlCl have been reported (29), but TlBr remains to be investigated. Also an analysis of the energy distribution of photoemitted electrons from these materials would give information on the density of electron states in the energy bands and would aid in the energy placement of the upper bands of the materials.

Energy loss measurements on fast electrons inelastically scattered from these crystals can be correlated with the optical measurements made here. Measurements of this type would be the most conclusive means of placing the value of the plasma resonance energy of electrons in the conduction band. Energy loss measurements have been made on the alkali halides (36) and on semiconducting materials (37) and give results in good agreement with optical work on these materials.

General recommendations can be made for improving the experimental apparatus constructed for this research. The light source and power supply should be redesigned to give better stability and higher intensity. An improved light source would result in a better signal-to-noise ratio and would result in more precise measurements. Vacuum conditions in the sample chamber should also be improved. Since reflectivity measurements are primarily limited to the surface of a material, a better vacuum would give a more stable surface and allow for controlled contamination experiments.

APPENDIX A

FRESNEL'S LAWS OF REFLECTION

The reflection of electromagnetic radiation occurs at a region in which an abrupt change takes place in the index of refraction. The mathematical laws of reflection may be derived by applying appropriate boundary conditions to the electric and magnetic field of the radiation.

Consider plane-polarized radiation incident on a semi-infinite plane interface between two media having permeabilities μ, μ', and permittivities ε, ε'. The plane interface is the $z = 0$ plane, and the wave is incident from the μ, ε medium. (See Figure 21). The boundary conditions applicable are

(1) continuity of the normal components of $\vec{D}$ and $\vec{B}$ of the incident wave at the boundary, and

(2) continuity of the tangential components of $\vec{E}$ and $\vec{H}$ at the boundary.

In order to satisfy these boundary conditions, both a reflected wave and a refracted wave must be present.

The waves may be represented by the following expressions:

$$\left.\begin{aligned} \vec{E} &= \vec{E}_o \, e^{i\vec{k} \cdot \vec{x} - i\omega t} \\ B &= \sqrt{\mu\varepsilon} \, \frac{\vec{k} \times \vec{E}}{k} \end{aligned}\right\} \qquad (22)$$

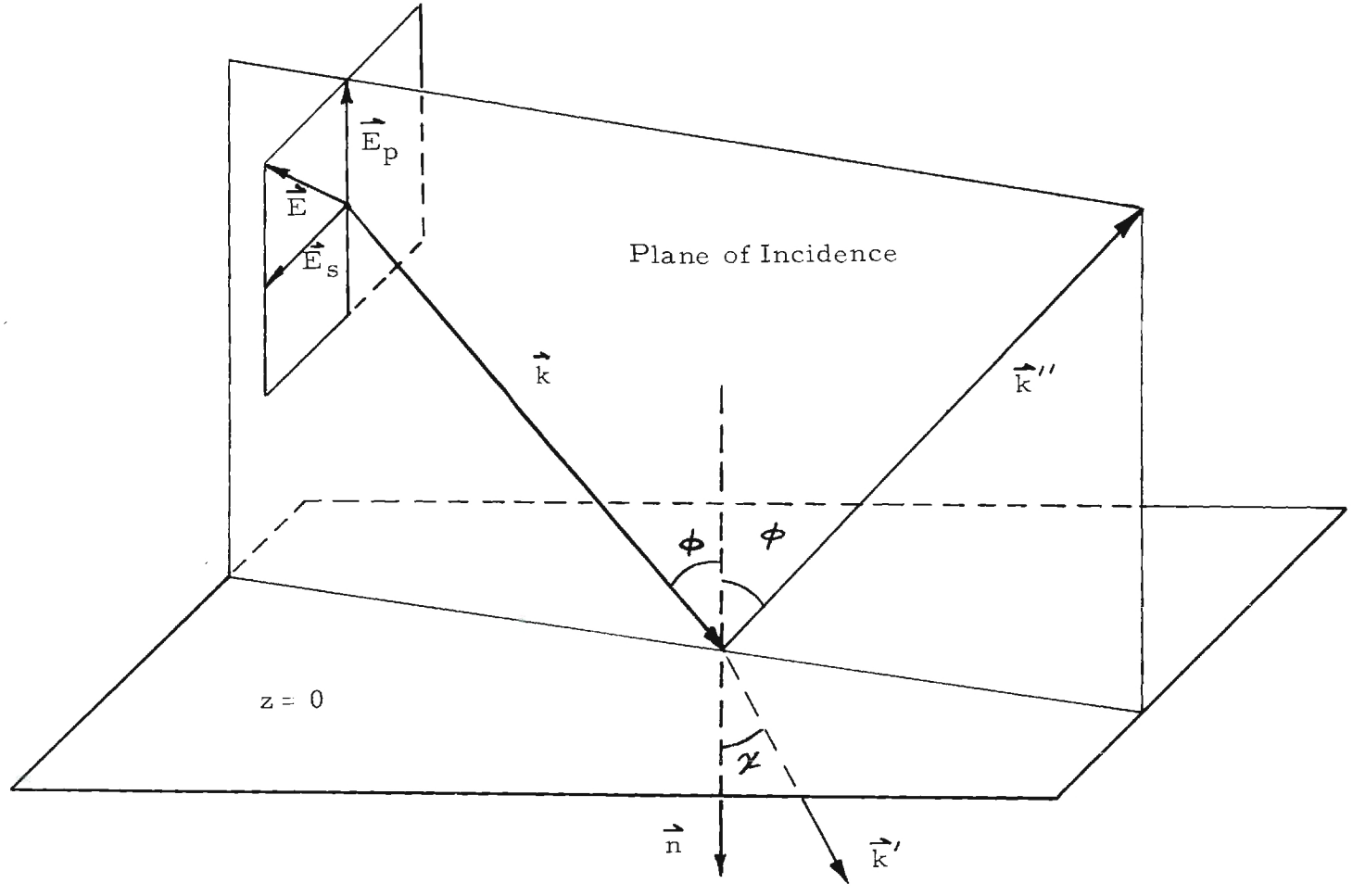

Figure 21. Optical Reflection Diagram.

$$\vec{E}' = \vec{E}_o' \, e^{i\vec{k}' \cdot \vec{x} - i\omega t}$$

$$\vec{B}' = \sqrt{\mu'\varepsilon'} \; \frac{\vec{k}' \times \vec{E}'}{k'} \tag{23}$$

$$\vec{E}'' = \vec{E}_o'' \, e^{i\vec{k}'' \cdot \vec{x} - i\omega t}$$

$$\vec{B}'' = \sqrt{\mu\varepsilon} \; \frac{\vec{k}'' \times \vec{E}''}{k''} \tag{24}$$

in which the single primes represent the refracted wave and the double primes represent the reflected wave. $\vec{k}$ is the wave vector, and the wave numbers have the magnitudes

$$|\vec{k}| = |\vec{k}''| = k = \frac{\omega}{c}\sqrt{\mu\varepsilon} \tag{25}$$

and

$$|\vec{k}'| = k' = \frac{\omega}{c}\sqrt{\mu'\varepsilon'} \tag{26}$$

where ω is the angular frequency of the wave.

The existence of boundary conditions which must be satisfied at all points on the plane $z = 0$ at all times implies that the spatial and time variation of all fields must be the same at $z = 0$. Consequently, the phase factors must all b e equal at $z = 0$, which implies the equalities

$$(\vec{k} \cdot \vec{x})_{z=0} = (\vec{k}' \cdot \vec{x})_{z=0} = (\vec{k}'' \cdot \vec{x})_{z=0} \tag{27}$$

independent of the nature of the boundary conditions. To satisfy equation (27) all three wave vectors must lie in a plane. Furthermore, the relations

$$k \sin \varphi = k' \sin \chi = k'' \sin \varphi_R$$

must hold. Since the wave vectors $\vec{k}''$ and $\vec{k}$ are equal, the angle of incidence φ is equal to the angle of reflection φ_r, which is the well-known law of reflection.

Snell's Law,

$$\frac{\sin \varphi}{\sin \chi} = \frac{k'}{k} = \sqrt{\frac{\mu' \varepsilon'}{\mu \varepsilon}} = \frac{n'}{n} , \tag{28}$$

in which n and n' are the refractive indices of the two media, is also derived from equation (27).

If the boundary conditions listed above are applied, the following equations result:

$$[\varepsilon(\vec{E}_o + \vec{E}_o'') - \varepsilon' \vec{E}_o'] \cdot \vec{n} = 0 \tag{29}$$

$$[\vec{k} \times \vec{E}_o + \vec{k}'' \times \vec{E}_o - \vec{k}' \times \vec{E}_o'] \cdot \vec{n} = 0 \tag{30}$$

$$(\vec{E}_o + \vec{E}_o'' - \vec{E}_o') \times \vec{n} = 0 \tag{31}$$

$$\left[\frac{1}{\mu} (\vec{k} \times \vec{E}_o + \vec{k}'' \times \vec{E}_o'') - \frac{1}{\mu'} (\vec{k}' \times \vec{E}_o') \right] \times \vec{n} = 0 . \tag{32}$$

In applying these boundary conditions, two separate situations can be considered, one in which the incident plane wave is linearly polarized with its electric field vector perpendicular to the plane of incidence, and the other in which the electric field vector is parallel to the plane of incidence. The general case of arbitrary elliptic polarization can be obtained by appropriate linear combinations of the two results.

First consider the electric field perpendicular to the plane of

incidence. Since the electric fields are all parallel to the surface, the first boundary condition in equation (29) yields nothing. Equations (31) and (32) give

$$E_o + E_o'' - E_o' = 0 \tag{33}$$

and

$$\sqrt{\frac{\varepsilon}{\mu}}\ (E_o - E_o'')\ \cos\varphi - \sqrt{\frac{\varepsilon'}{\mu'}}\ E_o' \cos\chi = 0\,, \tag{34}$$

while equation (30), using Snell's Law, duplicates equation (31). The relative amplitude of the reflected wave can be found from equations (33) and (34). It is

$$\frac{E_o'}{E_o''} = \frac{1 - \dfrac{\mu \tan\varphi}{\mu' \tan\chi}}{1 + \dfrac{\mu \tan\varphi}{\mu' \tan\chi}} \longrightarrow - \frac{\sin(\varphi - \chi)}{\sin(\varphi + \chi)}\,. \tag{35}$$

The expression on the right is the result appropriate when the permeabilities of the two media are equal, as is generally true for optical frequencies.

If the electric field is parallel to the plane of incidence the boundary conditions involved are normal $\vec{D}$, tangential $\vec{E}$, and tangential $\vec{H}$ (equations (29), (31), and (32)). The continuity of tangential $\vec{E}$ and $\vec{H}$ demand the results

$$\cos\varphi\ (E_o - E_o'') - \cos\chi\ E_o' = 0 \tag{36}$$

and

$$\sqrt{\frac{\varepsilon}{\mu}}\ (E_o + E_o'') - \sqrt{\frac{\varepsilon'}{\mu'}}\ E_o' = 0\,. \tag{37}$$

The continuity of normal $\vec{D}$, in addition to Snell's Law, merely duplicates equation (30). The relative amplitudes of the reflected electric field is then

$$\frac{E_o''}{E_o} = \frac{\frac{\mu}{\mu'} \sin 2\varphi - \sin 2\chi}{\sin 2\chi + \frac{\mu}{\mu'} \sin 2\varphi} \longrightarrow \frac{\tan(\varphi - \chi)}{\tan(\varphi + \chi)} . \qquad (38)$$

Again the result on the right applies for $\mu' = \mu$.

The reflecting power of the interface is defined as the ratio of the intensity of the reflected wave to the intensity of the incident wave. From equations (35) and (38) the reflecting power for light polarized perpendicular to the plane of incidence and parallel to the plane of incidence is then given by

$$r_s = \frac{\sin^2(\varphi - \chi)}{\sin^2(\varphi + \chi)} \qquad (39)$$

and

$$r_p = \frac{\tan^2(\varphi - \chi)}{\tan^2(\varphi + \chi)} \qquad (40)$$

APPENDIX B

COMPUTER PROGRAMS

Kramers-Kronig Computer Program

The integral to be evaluated

$$\theta(\omega_o) = \frac{1}{\pi}\int_o^\infty \ell n \left|\frac{\omega + \omega_o}{\omega - \omega_o}\right| \frac{d}{d\omega} \ell n\ r(\omega)\ d\omega \tag{41}$$

can be integrated by parts, and with a change of variable from ω to $E = \hbar\omega$ it assumes the form

$$\theta(E') = \frac{E'}{\pi}\int_o^\infty \frac{\ell n\ r(E) - \ell n\ r(E')}{E^2 - E'^2}\, dE \tag{42}$$

$$= \frac{E'}{\pi}\int_o^\infty Y(E, E')\, dE\ . \tag{43}$$

Employing the trapezoidal rule, the integral can be approximated as

$$\theta(E') = \frac{E'}{2\pi}\sum_{n=o}^{N} (Y_{n+1} - Y_n)(E_{n+1} - E_n), \tag{44}$$

where $Y_n = Y(E', E_n)$.

For a calculation of the optical constants of a material from its reflectivity, N energies are chosen whose corresponding values of $r(E)$ give a good approximation to the reflectivity curve when connected by straight lines. The computer program then evaluates a different set of

Y_n's for each E' from the set of E_n's and sums them by equation (44) to give $\theta(E')$. Since E_n and E' in equation (42) both come from the same set, the singularity that occurs when $E_n = E'$ can be handled by taking the derivative of the numerator and the denominator of equation (42):

$$Y(E_n, E_n) = \frac{[dr(E)/dE]_{E = E_n}}{2 E_n r(E_n)} . \tag{45}$$

This expression can be approximated by

$$Y(E_n, E_n) = \frac{r(E_{n+1}) - r(E_{n-1})}{2E_n r(E_n)(E_{n+1} - E_{n-1})} . \tag{46}$$

If E_n happens to correspond to a peak in the reflectivity spectrum, $Y(E_n, E_n)$ must equal zero. Thus the values of $r(E_{n+1})$ and $r(E_{n-1})$ must be chosen at the proper energy to give equal r's. This can easily be done in choosing the set of E values to be used as input. The computer program chooses the proper expression, (42) or (46), to evaluate each $Y(E', E_n)$.

Next n, k, and α are computed from the values of E', $r(E')$, and $\theta(E')$ from equations (2), (13), and (14). The program prints out each E' and its corresponding n, k, and α, along with $\theta(E')$ for possible diagnostic purposes. The program, written in the extended Algol language for the Burroughs B-5500 computer, is reproduced below.

```
            BEGIN
COMMENT         ENERGY DEPENDENCE OF OPTICAL CONSTANTS N AND K AND
                ABSORPTION COEFFICIENT ALPHA FROM A KRAMERS-KRONIG
                ANALYSIS OF THE REFLECTIVITY SPECTRUM OF A MATERIAL  ;
FILE IN         CARD (2,10)  ;
FILE OUT        LINE 6 (2,15)  ;
FORMAT OUT      TITLE(X2,"ENERGY",X7,"N",X7,"K",X7,"ALPHA",/),
                RESULTS(X3,F6.2,X6,F5.3,X3,F5.3,X3,F8.3,X5,F10.5)  ;
REAL            SUM, D  ;
INTEGER         I, J, A, B  ;
ARRAY           R, E, X, U, N, K, CO, Y, THETA[0:250]  ;
LIST            DATA ( A, B, FOR I ← 0 STEP 1 UNTIL A DO
                [ E[I], R[I] ] )  ;
                WRITE (LINE, TITLE)  ;
                READ(CARD,/,DATA)  ;
                FOR I ← 0 STEP 1 UNTIL A      DO
            BEGIN
                R[I] ← 0.01×R[I]  ;
                X[I] ← LN( R[I] )  ;
                U[I] ← SQRT( R[I] )
            END  ;
                FOR J ← 0 STEP 1 UNTIL A - 55     DO
            BEGIN
                FOR I ← 0 STEP 1 UNTIL A      DO
                IF I = J THEN Y[I] ← ( R[I+1] - R[I-1] ) / ( 2×E[I]×R[I]×
                                    ( E[I+1] - E[I-1] ) )      ELSE
                Y[I] ← ( X[I] - X[J] ) / ( E[I]↑2 - E[J]↑2 )  ;
                SUM ← Y[A]×E[A] - Y[0]×E[0]  ;
                FOR I ← 0 STEP 1 UNTIL A-1      DO
                SUM ← SUM + Y[I]×E[I+1] - Y[I+1]×E[I]  ;
                THETA[J] ← 0.159×E[J]×SUM  ;
                D ← 1 + R[J] - 2×U[J]×COS(THETA[J])  ;
                N[J] ← ( 1 - R[J] ) / D  ;
                K[J] ← 2×U[J]×SIN(THETA[J]) / D  ;
                CO[J] ← ( 1.513 E5 )×K[J]×E[J]
            END.
```

Fresnel Curve-Fitting Computer Program

In order to select the proper values of n, k, and ρ_m from an experimentally determined curve of reflectivity versus angle of incidence, a curve is calculated from the combination of equations (7) and (8) for a given set n, k, ρ_m from a previously determined range, and the mean square deviation of this curve from the experimental curve is calculated by the computer. The computer then prints the value of n, k, ρ_m, and the deviation for that set. The proper n, k, and ρ_m are then selected by simply choosing the smallest deviation.

The computer program, written for the B-5500 computer, contains a test procedure to immediately discard a set of values n, k, and ρ_m if the first calculated point misses the first experimental point by more than a given value. A program was also written for the Burroughs B-220 computer to print out the best fit curve for a given n, k, and ρ_m. The curve-fitting program is reproduced below.

```
          BEGIN
COMMENT         CALCULATION OF OPTICAL CONSTANTS BY CURVE-FITTING FRESNEL
                EQUATIONS TO EXPERIMENTAL CURVE OF REFLECTANCE VERSUS
                ANGLE OF INCIDENCE   ;
FORMAT DUI      TITLE (X10,"N",X10,"K",X9,"RHO",X6,"RMS DEVIATION",/) ,
                IDENT (X55,F7.1,6(F6.1))   ,
                RESULTS(X8,F5.3,X6,F5.3,X6,F5.3,X3,F11.6)   ;
LABEL           EXIT, START   ;
REAL ARRAY      R, C, S, T[0:30]   ;
INTEGER         I   ;
REAL            N, K, X, Y, A, B, D, WRMS, RMS, RS, RP, RHO, F, G, L, M,
                E, H, J, U, V, P, Q, RT, ID   ;
LIST            DATA ( L, M, F, P, Q, G, E, H, J, U, ID, FOR I ← 0 STEP 1
                      UNTIL 20 DO R[I] )   ;
LIST            CONSTANTS ( FOR I ← 0 STEP 1 UNTIL 20     DO
                          [ C[I], S[I], T[I] ] )   ;
LIST            RANGE (ID, L, F, P, G, E, J)   ;
                WRITE (LINE,TITLE)   ;
                READ (CARD,/,CONSTANTS)   ;
START:          READ (CARD,/,DATA)[EXIT]   ;
                WRITE (LINE, IDENT, RANGE)   ;
                V ← U/21.0   ;
                FOR N ← L STEP M UNTIL F     DO
          BEGIN
                FOR K ← P STEP Q UNTIL G     DO
          BEGIN
                FOR RHO ← E STEP H UNTIL J     DO
          BEGIN
                WRMS ← 0.0   ;
                FOR I ← 2 STEP 1 UNTIL 20     DO
          BEGIN
                X ← N*2 - K*2 - S[I]*2   ;
                Y ← SQRT( X*2 + 4×(N×K)*2 )   ;
                A ← 0.707×SQRT(Y + X)   ;
                B ← 0.707×SQRT(Y - X)   ;
                U ← A*2 + B*2   ;
                RS ← (D - 2×A×C[I] + C[I]*2)/(D + 2×A×C[I] + C[I]*2)   ;
```

```
            RP ← RS×(D - 2×A×S[I]×T[I] + (S[I]×T[I])*2)/(D +
                       2×A×S[I]×T[I] + (S[I]×T[I])*2)   ;
            RT ← ( RP + RHO×RS ) / ( RHO + 1.0 )   ;
            RMS ← ( R[I] - RT )*2   ;
            WRMS ← WRMS + RMS   ;
            IF WRMS > U + ( I - 22 )×V THEN BEGIN
            I ← 20   ;
            WRMS ← 1.0      END   ;
        END ;
            IF WRMS < 0.00005      THEN
            WRITE (LINE, RESULTS, N, K, RHO, 10000×WRMS)   ;
        END
        END
        END ;
            GO TO START   ;
EXIT:       END.
```

BIBLIOGRAPHY

1. J. C. Phillips, "The Fundamental Optical Spectra of Solids," in Solid State Physics (ed. F. Seitz and D. Turnbull), Vol. 18: Academic Press, New York, 1966.

2. L. I. Korovin, Fizika Tverdoga U.S.S.R. 1, 1311 (1959) [translation: Soviet Physics - Solid State 1, 1202 (1960)].

3. F. C. Jahoda, Physical Review 107, 1261 (1957).

4. H. J. Bowlden and J. K. Wilmshurst, Journal of the Optical Society of America 53, 1073 (1963).

5. H. R. Phillip and E. A. Taft, Phys. Rev. 136, A 1445 (1964).

6. K. Ishiguro and T. Sasaki, Scientific Papers of the College of General Education of the University of Tokyo 12, 19 (1962).

7. R. Tousey, J. Opt. Soc. Am. 29, 235 (1939).

8. I. Simon, J. Opt. Soc. Am. 41, 336 (1951).

9. W. R. Hunter, J. Opt. Soc. Am. 55, 1197 (1965).

10. T. Sasaki and K. Ishiguro, Japanese Journal of Applied Physics 2, 289 (1963).

11. H. R. Phillip and E. A. Taft, Phys. Rev. 113, 1002 (1959).

12. W. C. Walker and J. Osantowski, Phys. Rev. 134, A 153 (1964).

13. H. R. Phillip and H. Ehrenreich, Phys. Rev. 131, 2016 (1963).

14. M. Cardona and D. L. Greenaway, Phys. Rev. 133, A 1685 (1964).

15. H. Ehrenreich, H. R. Phillip, and J. C. Phillips, Physical Review Letters 8, 59 (1962).

16. H. Zinngrebe, Zeitschrift für Physik 154, 495 (1959).

17. W. Martienssen, Journal of the Physics and Chemistry of Solids 8, 294 (1959).

18. S. Tutihasi, J. Phys. Chem. Solids 12, 344 (1960).

19. I. Lefkowitz, R. P. Lowndes, and A. D. Yoffe, J. Phys. Chem. Solids 26, 1171 (1965).

20. N. F. Mott, Proceedings of the Royal Society, A167, 384 (1938).

21. P. D. Johnson, J. Opt. Soc. Am. 42, 278 (1952).

22. G. Hass, W. R. Hunter, and R. Tousey, J. Opt. Soc. Am. 50, 862 (1960).

23. A. Smith, J. Opt. Soc. Am. 50, 862 (1960).

24. R. A. Knapp, Applied Optics 2, 1334 (1963).

25. K. Watanabe and E. C. Y. Inn, J. Opt. Soc. Am. 43, 32 (1953).

26. D. C. Hinson, J. Opt. Soc. Am. 56, 408 (1966).

27. A. Smakula and M. W. Klein, J. Opt. Soc. Am. 40, 748 (1950).

28. F. W. Barth, American Mineralogist 14, 358 (1929).

29. T. Yanagi, Journal of the Physical Society of Japan 18, 1552 (1963).

30. H. Ehrenreich and H. R. Phillipp International Conference on Semiconductor Physics, Exeter, 1962: Adlard and Son, Ltd., London, 1962.

31. L. Marton, Reviews of Modern Physics 28, 172 (1956).

32. C. J. Powell, Proceedings of the Physical Society (London) 76, 593 (1960).

33. P. Nozieres and D. Pines, Phys. Rev. 113, 1254 (1959).

34. J. A. Bearden and A. F. Burr, U. S. Atomic Energy Commission Report NYO-2543-1.

35. D. M. Roessler, British Journal of Applied Physics 16, 1119 (1965).

36. C. J. Powell, Proc. Phys. Soc. (London) 76, 593 (1960).

37. M. Creuzburg and H. Raether, Solid State Communications 2, 345 (1964).

VITA

David Chandler Hinson was born in Millen, Georgia in April 17, 1939, the son of Dr. and Mrs. Conrad R. Hinson. He was educated in the public schools of Bennettsville, South Carolina, and was graduated from the Bennettsville High School as valedictorian of the Class of 1957. He entered the Georgia Institute of Technology in 1957 and received the B.S. degree, with honor, in Physics in 1961 and the M. S. degree in Physics in 1964.

During his graduate study he has held Graduate Teaching and Research Assistantships in the School of Physics. He is a member of Delta Sigma Phi social fraternity, the Society of Sigma Xi, and Phi Kappa Phi, Tau Beta Pi, Sigma Pi Sigma, and Phi Eta Sigma honorary fraternities. He is a member of the American Physical Society and the Optical Society of America.

He is married to the former Anne Harvey McMichael of Atlanta, and they have three children.